CAPITAL UNIVERSITY OF SCIENCE AND TECHNOLOGY, ISLAMABAD

Preparation and Optimization of pH Driven Pluronic Micelles-based Drug Delivery Carrier for the Treatment of Intestinal Inflammatory Disease

by

Aqeela Zahra

A thesis submitted in partial fulfillment for the degree of Master of Science

in the

Faculty of Pharmacy
Department of Pharmacy

2025

With utmost love and respect, I dedicate this modest effort to our beloved Prophet Hazrat Muhammad (Peace Be Upon Him), the greatest teacher and mercy for all of mankind who was commanded first: "Iqra'-Read!"(Surah Al-'Alaq, 96:1). May this work in a small way assist in that noble pursuit of learning which He set forth so beautifully.

CERTIFICATE OF APPROVAL

Preparation and Optimization of pH Driven Pluronic Micelles-based Drug Delivery Carrier for the Treatment of Intestinal Inflammatory Disease

by

Aqeela Zahra

(MPH233013)

THESIS EXAMINING COMMITTEE

S. No.	Examiner	Name	Organization
(a)	External Examiner	Dr. Gul Shahnaz	QAU, Islamabad
(b)	Internal Examiner	Dr. Nadia Shamshad Malik	CUST, Islamabad
(c)	Supervisor	Dr. Mahira Zeeshan	CUST, Islamabad

Dr. Mahira Zeeshan
Thesis Supervisor
October, 2025

Dr. Nadia Shamshad Malik
Head
Department of Pharmaceutics
October, 2025

Dr. Muzaffar Abbass
Dean
Faculty of Pharmacy
October, 2025

Author's Declaration

I, **Aqeela Zahra** hereby state that my M.Phil thesis titled "**Preparation and Optimization of pH Driven Pluronic Micelles-based Drug Delivery Carrier for the Treatment of Intestinal Inflammatory Disease**" is my own work and has not been submitted previously by me for taking any degree from Capital University of Science and Technology, Islamabad or anywhere else in the country/abroad.

At any time if my statement is found to be incorrect even after my graduation, the University has the right to withdraw my M.Phil Degree.

(Aqeela Zahra)

Registration No: MPH233013

Plagiarism Undertaking

I solemnly declare that research work presented in this thesis titled "**Preparation and Optimization of pH Driven Pluronic Micelles-based Drug Delivery Carrier for the Treatment of Intestinal Inflammatory Disease**" is solely my research work with no significant contribution from any other person. Small contribution/help wherever taken has been duly acknowledged and that complete thesis has been written by me.

I understand the zero tolerance policy of the HEC and Capital University of Science and Technology towards plagiarism. Therefore, I as an author of the above titled thesis declare that no portion of my thesis has been plagiarized and any material used as reference is properly referred/cited.

I undertake that if I am found guilty of any formal plagiarism in the above titled thesis even after award of M.Phil Degree, the University reserves the right to withdraw/revoke my M.Phil degree and that HEC and the University have the right to publish my name on the HEC/University website on which names of students are placed who submitted plagiarized work.

(Aqeela Zahra)

Registration No: MPH233013

Acknowledgement

First of all, I thank **Allah Almighty** for His endless blessings, mercy, wisdom, guidance, and strength without which this work would not have been possible.

I am especially thankful to my **Ammi and Abu Jee** whose prayers, love, and lifelong support have led the way to all of my achievements.

I would like to express my sincere gratitude to my **supervisor Dr. Mahira Zeeshan** for her guidance, feedback, and encouragement that helped steer the direction of this research work.

I also appreciate all the support from my respected teachers, **Dr. Muzaffar Abbas** and **Dr. Nadia Shamshad**, who enriched my coursework.

I would like to express special thanks to my friend **Dr. Shazia Siddique** for her moral support and constant motivation during difficult times, as well as to my colleagues **Dr. Muhammad Muddassir** and **Mr. Naseeb Gul**, whose contribution made this academic journey fruitful. Finally, I would also like to thank all of my friends and colleagues who have been a source of strength and joy throughout the course of my studies.

(Aqeela Zahra)

Abstract

The chronic inflammation, poor bioavailability of conventional agents, and the absence of site-specific delivery systems make inflammatory bowel disease (IBD) a major therapeutic challenge. In this study a pH-responsive nanocarrier was developed by formulating silymarin-loaded pluronic micelles coated with Eudragit® S100 (SLM-ES-PLU-Ms) for colon-targeted drug release in prolonged time. The formulation was optimized using a Box-Behnken design, which yielded nanosized micelles (∼42 nm) with a uniform distribution (PDI 0.18), high encapsulation efficiency (79.63%), and a stable negative surface charge (-42 mV).

Physicochemical analyses, Scanning Electron Microscopy (SEM), Attenuated Total Reflectance-Fourier Transform Infrared spectroscopy (ATR-FTIR), and X-ray Powder Diffraction (XPRD) confirmed the successful entrapment of the drug and the structural stability of the micelles. In vitro release studies indicated pH-selective performance, showing minimal drug release at gastric pH (5.03% at pH 1.2) and sustained release under colonic conditions (99.08% at pH 7.4 over 72 hours). The release kinetics were optimally described by the Peppas-Sahlin model, suggesting that transport is driven by diffusion transport mechanism.

The therapeutic efficacy was assessed using a mouse model of Dextran sodium sulfate (DSS) induced colitis. Animals administered SLM-ES-PLU-Ms demonstrated notable enhancements in disease activity index, preservation of colon length, and histological scores in comparison to free silymarin (SLM) and untreated controls. These findings indicate that SLM-ES-PLU-Ms successfully address the solubility and bioavailability challenges associated with SLM, providing a stable platform for colon specific targeted delivery. This nanocarrier system demonstrates significant potential for application as a novel therapeutic approach in ulcerative colitis and associated intestinal inflammatory conditions.

Contents

List of Figures

List of Tables

Abbreviations

ATR-FTIR	Attenuated Total Reflectance - Fourier Transform Infrared Spectroscopy
CD	Crohn's Disease
CMC	Critical Micelles Concentration
CMT	Critical Micelles Temperature
COX-2	Cyclooxygenase-2
DDS	Drug Delivery System
DL	Drug Loading
DSS	Dextran Sodium Sulfate
EE	Encapsulation Efficiency
EPR	Enhanced Permeability and Retention Effect
FDA	Food and Drug Administration
GIT	Gastrointestinal Tract
HLB	Hydrophilic Lipophilic Balance
IBD	Inflammatory Bowel Disease
IFN	Interferon
IL	Interleukin
iNOS	Inducible Nitric Oxide Synthase
NF-κB	Nuclear Factor κB
NPs	Nanoparticles
PDI	Polydispersity Index
PEO	Poly (ethylene oxide)
PGE-2	Prostaglandin E2
PMs	Polymeric Micelles

PPO	Poly (propylene oxide)
ROS	Reactive Oxygen Species
SLM	Silymarin
TGF	Transforming Growth Factor
TNF	Tumor Necrosis Factor
UC	Ulcerative Colitis

Symbols

Γ	Surface tension (in equations)
λmax	Wavelength of maximum absorbance

Chapter 1

Introduction

1.1 Background of the Study

Inflammatory bowel disease (IBD) is a chronic, episodic condition characterized by mucosal inflammation of the gastrointestinal tract (GIT), primarily affecting the colon and ileum [1]. The two most common forms of IBD are Crohn's disease (CD) and ulcerative colitis (UC). The primary distinction between the two forms is the location and depth of inflammation of the gut. The innermost mucosal layer, which runs continuously from the rectum to the proximal colon, is impacted by inflammation in UC. Inflammation in CD spreads to deeper tissues and can occur in any GI segment, most frequently in the colon and terminal ileum, in a discontinuous fashion [1]. High morbidity, a lower quality of life and an elevated risk of colorectal cancer are linked to UC and CD. Over the past twenty years, the global landscape of IBD has undergone a profound transformation. Once considered a condition largely confined to Western industrialized nations (North America, Western Europe), IBD has emerged as a significant and rapidly growing health challenge in newly industrialized countries and regions undergoing rapid economic development. This shift is characterized by a dramatic increase in both the incidence (number of new cases per year) and prevalence (total number of cases in a population) of CD and UC in nations across Asia, South America, and the Middle East [2]. The incidence of IBD has increased globally in tandem with the expansion of global industrialization, placing a significant load

on public healthcare [3]. An estimated 1.4 million people in the US and 2.2 million in Europe are thought to have IBD, and the number is rising quickly. Furthermore, epidemiological crossroads of numerous Western diseases have been observed in Asian nations throughout the past 20 years.

India is now predicted to have the largest IBD disease burden of 1.4 million patients. IBD prevalence is sharply rising in both industrialized and developing nations as a result of the increased demand for modern lifestyles [4].

Although IBD etiology has been investigated, the underlying causes are still unclear. Multiple factors frequently contribute to the development of IBD. It is believed that microbial exposure, endogenous triggers such as genetic predisposition and immunoregulatory dysfunction, and external environmental triggers including nutrition, chemicals, and psychological stress played a role in the development of IBD.

Recent research on the human microbiome has suggested that dysbiosis, or a shift in the usual makeup of the microbiota, plays a key role in the development of IBD [2]. A genetically predisposed person's ongoing inflammatory response to endogenous microorganisms also paved way towards IBD. [5]. In short, IBD is caused by a complex interaction of immunologic, genetic, and environmental factors [5].

Furthermore, research studies highlighted the importance of gut microbiota in the pathogenesis of IBD Dysbiosis, characterized by decreased diversity and the overabundance of pathogenic taxa, including Enterobacteriaceae, ultimately results in immune dysregulation and chronic inflammation [2].

Dysbiosis is challenging for oral drug delivery, since these changes will affect pH, enzymes, and mucosal permeability, and thus limit the efficacy of conventional drugs.

Consequently, oral drugs have limited utility for patients with IBD; different strategies have been opted to deliver drugs through the oral route by overcoming GIT barriers, like drug encapsulation inside the pH-responsive nanocarriers and micelles to selectively release the drug in the inflamed colon [6].

The most typical symptoms of IBD include weight loss, diarrhea, stomach pain, and fluid loss.

The IBD recurrence rate is about 50–80%. Therefore, long-term protection is necessary from IBD recurrence, which raises the expenditures. Severe immunological responses in the gut epithelium are part of the disease pathophysiology, especially in genetically susceptible individuals.

Based on the evolving circumstances of cultures around the world, IBD has four stages: inception, acceleration in incidence, compounding prevalence, and prevalence equilibrium [7].

IBD has a wide prevalence in Europe and the United States. It has now spread worldwide with an increasing prevalence in recently industrialized nations in Asia, South America, and the Middle East [8]. IBD, which was once thought to be a condition that only affected adolescents and young adults, is now more frequently seen in older people [9].

Its incidence is increasing among children and older adults in developed nations. IBD has a significant impact on patients' quality of life and the healthcare system; hospitalization rates range from 8.2 to 17 per 100,000 people annually, and treatment expenses total $6.8 billion annually [10].

IBD is characterized by abnormal intestinal permeability, increased immune cell infiltration, and increased mucus production. Altered synthesis and release of pro-inflammatory cytokines (interleukin (IL)-1, IL-6, and IL-12), tumor necrosis factor (TNF), interferon (IFN), transforming growth factor (TGF), and elevated reactive oxygen species (ROS) are the factors that contribute to intestinal inflammation and cause excessive damage to intestinal tissues [10].

Conventional treatment methods work by healing the mucosal and exacerbated inflammation and moderating the systemic immune responses [10].

The condition can be managed with a variety of pharmacological therapies, such as biologics, corticosteroids, immunosuppressants, and aminosalicylates. However, drugs therapeutic efficacy is limited by their pharmacokinetic constraints, side effects, drug resistance, increased cost, and poor patient compliance. Many pathophysiological barriers, such as degradation by the gastric pH, GI enzymes or biliary fluid, first pass

effect and rapid clearance due to heavy diarrhea inherent in UC, make oral delivery of therapeutic agents, the most practical and direct route to the inflamed gastrointestinal tract (GIT), less effective at crossing the mucus layer [11].

Natural phytochemicals with anti-inflammatory and antioxidant properties, such as flavonoids and phenolic compounds, have been used in IBD. They alter a number of inflammatory mediators, including cyclooxygenase-2 (COX-2), prostaglandin E2 (PGE-2), inducible nitric oxide synthase (iNOS), IL-1, IL-6, IL-10, and TNF-α. Furthermore, the ability of natural macromolecules to inhibit the biochemical and molecular inflammatory processes linked to IBD is also evaluated. Several in vitro and in vivo studies have recently suggested that the antioxidant and anti-inflammatory properties of bio-phenols obtained from fruits and vegetables are advantageous to combat IBD [9].

For instance, silymarin (SLM) is a polyphenolic substance derived from milk thistle seeds that contains flavonoids and flavonolignans [12]. Known by its botanical name, Silybum marianum L., it is a well-known flavonolignan that belongs to the Asteraceae family and was once one of the most commonly used drugs. SLM is well known for its anti-inflammatory, anti-diabetic, anti-nociceptive, anti-cancer, hepatoprotective, and maybe anti-oxidative properties. SLM's poor solubility poses a significant obstacle to its bioavailability; its oral administration leads to 23–47% absorption of the substance [13].

Numerous conditions, including cancer, non-alcoholic fatty liver disease, inflammatory bowel illnesses, and chronic liver diseases, can benefit from SLM. Even though silymarin has been shown to be safe and beneficial in preclinical and clinical research, its limited intestinal absorption, low bioavailability, and poor water solubility limit its clinical relevance. The application of formulation development and nanotechnology methods seems to be a promising strategy to get around these biopharmaceutical limits and enhance its therapeutic potential [12].

Silybum marianum seeds yield a bioactive chemical called silymarin, which has strong anti-inflammatory properties. The main active ingredient in silymarin, silibinin, is a combination of two diastereomers that contain silibinin A and silibinin B in almost

equal amounts. By focusing on many stages of the viral replication cycle, SLM has demonstrated potent antiviral properties against a variety of viral agents. Its hepatoprotective properties are widely known. By supporting the reduction of bowel inflammatory cytokines, particularly TNF-α, interleukin-1β (IL-1β), and nuclear factor κB (NF-κB), and repairing the bowel histology in vitro, several studies have proven that silymarin has a unique effect on the control of immune-based murine colitis [7].

Various polymer and surfactant-based carrier systems have been devised to deliver the drug safely to the inflamed gut. The low Critical Micelles Concentration (CMC) values, strong biocompatibility profile, and high drug entrapment effectiveness of polymeric surfactants, which have a large hydrophobic inner core, make them a safer and more practical substitute for traditional surfactants. Pluronics or Poloxamers, which are polyethylene oxide-polypropylene oxide block copolymers, are the most studied class of them. These FDA-approved surfactants are employed in a variety of nanocarriers, micelles, gels, and polymer-stabilized nano emulsions to increase the bioavailability and solubility of the active medicinal components that are poorly soluble in water. They are frequently utilized as a carrier for controlled drug delivery because of their unique tri-block copolymer structure, which provides advantages in terms of modifying the release. Numerous investigations have proven that micellar carriers containing Pluronic polymers are biocompatible across a wide concentration range [14].

The amphiphilic nature of nanomicelles allows hydrophobic pharmaceuticals to be encapsulated within their core structure, improving drug solubilization. The simplicity of preparation, frequently achieved through straightforward self-assembly procedures, sets polymeric micelles apart from more intricate nanoparticle compositions. Additionally, their ability to release drugs in a controlled and prolonged manner enhances therapeutic effects [15].

Pluronic, a polymer and a surfactant, with varying molecular weights, has a wide range of applications in the pharmaceutical sector and drug administration because of its superior drug complexation ability and other appealing properties. To increase the stability, safety, bioavailability, and solubility of medicinal molecules, the pharmaceutical industry uses Pluronic. The Pluronic's middle portion (the hydrophobic

PPO group) is joined to the two hydrophilic PEO end groups [16]. In drug delivery applications, Pluronics are highly beneficial due to their amphiphilic character. Drugs can have their circulation duration prolonged by Pluronic. The FDA has approved the pharmaceutical component PLU for use in medicine. Additionally, the US and British pharmacopoeias classify it as a pharmaceutical excipient [16].

The triblock copolymer PLU is made up of poly (ethylene oxide) (PEO) and poly (propylene oxide) (PPO) blocks stacked in the PEO101-PPO56-PEO101 configuration. Because of its structure, PLU can micellize in aqueous solutions when the concentration goes beyond the critical micellization temperature (CMT) and surpasses the critical micelle concentration (CMC). PPO block length affects CMC; longer PPO blocks result in lower CMC values, which is important for the assembly and action of drug delivery systems. Its chemical and physical characteristics make it a perfect option for medication delivery.

For its pharmacological usage, its capacity to form stable micelles, solubilize hydrophobic medications, and thermosensitive behavior, such as gelling at body temperature, are essential. FDA approval of PLU highlighted its safety and biocompatibility in a range of formulations. It has been well documented that PLU successfully overcomes issues such as restricted bioavailability, pH degradation, and poor water solubility. A useful and adaptable polymer for medication delivery applications is PLU. Targeted drug distribution is made easier by its special composition and characteristics [17].

The presence of 70% PEO blocks in PLU is responsible for its hydrophilicity. In situ sol-gel transformations are made possible by PLU, which is stable, biocompatible, and non-toxic. These characteristics make PLU special in terms of drug delivery methods and uses [18].

Amphiphilic copolymers self-assemble in an aqueous solution to form nanoscale carriers known as polymeric micelles (PMs). They typically have an outer shell and a spherical inner core. Drug release from drug delivery carriers has been controlled by adjusting the pH values in the gastrointestinal (GI) tract, which range from 1 to 3 in the stomach to 6 to 7.5 in the small intestine. For oral medication delivery, pH-sensitive PMs have several benefits, such as preventing drug destruction in the

upper GI tract, enhancing drug solubilization, and releasing the drug in a spatially controlled manner [19].

Moreover, enteric-coated solid dosage forms have been prepared using commercially available pH-responsive materials, such as methacrylic acid copolymers (Eudragit®), which dissolve at a specific pH. These materials are generally safe. The pH-responsive properties of methacrylate copolymer-coated nanocarriers (ES) make them appropriate for drug release in the colon's higher pH environments [20]. Eudragit®, a pharmaceutical coating polymer that is soluble in alkaline conditions and resistant to acidic pH, was first launched in the international market in 1953. The pH-sensitive methacrylate polymer Eudragit® comes in a variety of forms that dissolve in varying pH ranges. Eudragit® targets many parts of the digestive system and comes in cationic, anionic, and neutral forms [21]. Methacrylic acid and methyl methacrylate anionic copolymers, like ES, are very pH-dependent. ES has been suggested for usage in microencapsulation for controlled-release applications because to its distinct pH-solubility profile. Since this polyacrylic resin is pH-sensitive and soluble at pH 7 or higher because carboxylic acid groups are present, it is suitable for medication targeting in the colon. A pH-responsive polymer called ES is used to effectively prevent ulcerative colitis [22].

The USA, Europe, and Japan have all approved the oral administration of ES. The polymer releases the drug that is encapsulated in the colon when it dissolves selectively in aqueous media with a pH of 6–7. Much of the encapsulated medication is released right away from ES loaded preparations as a result of the alteration in intestinal pH [23].

1.2 Epidemiological Shift and Regional Trends in IBD

In the last decade, IBD has experienced a rapid epidemiological transition, going from a Western disease to a global health issue. Recent data show that in South Asia, especially in India, Pakistan, and Bangladesh, the incidence has been increasing at

∼16.8% per year from 2010 to 2020. Urbanization, shifts toward processed foods, and the overuse of antibiotics are hypothesized to be causing these increases through the hygiene hypothesis and microbiome disruption.

In Pakistan, varying quality of data and frequent misclassification with diseases such as intestinal tuberculosis still belies the real burden of IBD. The emerging trends should underline the importance of improving regional surveillance systems and designing local-use treatment approaches, for example, colon-targeted nanocarriers.

1.3 Problem Statement

The frequent drug degradation due to pathophysiological barriers and clearance of SLM from diarrhea in IBD limits the effectiveness of the drug for intestinal inflammatory diseases, requiring repeated dosing that leads to systemic side effects. Despite being a promising phytoconstituent with anti-inflammatory properties, SLM has low oral bioavailability (BCS Class IV), poor aqueous solubility, and instability in the stomach environment. Its clinical effectiveness is compromised by these factors. Thus, it is necessary to develop a reliable and focused drug delivery system to improve SLM's therapeutic effectiveness in controlling intestinal inflammation and overcoming its pharmacokinetic limitations.

1.4 Objectives of the Study

1. Preparation of pH-driven Pluronic micelles-based drug delivery carrier system.
2. Optimization of formulation by using Design Expert®software.
3. Physicochemical and in vitro characterization of pH-driven Pluronic micelles-based drug delivery carrier system.
4. In vitro drug release studies and mathematical modelling to investigate drug release kinetics and mechanism.

5. In vivo animal studies on murine Dextran sodium sulfate (DSS) induced Colitis model to establish therapeutic efficacy.

1.5 Research Questions

1. Can SLM be efficiently encapsulated in Pluronic-based polymeric micelles to enhance its physicochemical stability and aqueous solubility?
2. Does the micellar formulation allow for sustained drug release in intestinal conditions and shield SLM from early gastric degradation?
3. Is the SLM-ES-PLU-Ms system successfully developed with the desired features?
4. Does the developed formulation show better anti-inflammatory activity in the in vivo intestinal inflammation models?

1.6 Significance of the Study

This study focused on developing a pH-sensitive Pluronic micelle-based drug delivery system to deliver SLM in a sustained manner while maintaining its stability and local bioavailability at the inflamed intestine for better therapeutic efficacy. By delivering targeted and sustained drug release at the site of inflammation in colon targeting for prolonged time, the formulation seeks to lower the frequency of dosing and systemic side effects. It provides a new, non-invasive treatment approach that may lead to better patient outcomes for the treatment of IBD.

1.7 Scope and Limitations

The primary objective of this research is to develop and characterize a SLM-loaded pH-sensitive PLU micellar formulation for its enhanced solubility, stability, and targeted delivery in IBD, which involves formulation preparation, optimization, in vitro and in vivo testing of anti-inflammatory potential. This study does not extend to comparative clinical efficacy, long-term toxicity, or human pharmacokinetics.

Chapter 2

Literature Review

2.1 IBD and the Role of SLM

IBD patients go through two stages in succession. One is the active disease phase, often known as the flare-up/relapse state, during which symptoms are most noticeable. The remission state, which is characterized by a time of silence and minimal symptoms, comes next. Abdominal pain, severe diarrhea, bloody stool, exhaustion, fever, and weight loss are the common symptoms. Anemia, skin issues, liver inflammation, bone weakening, and other intestinal and extraintestinal disorders could arise [1]. The primary issue in treating IBD is the intricacy of the disease and its multifaceted origin. Unfortunately, there is now no known cure for IBD; therefore, patients must rely on medication for the rest of their lives. The goals of IBD treatment are to relieve symptoms while the disease is active and to induce and sustain remission. The underlying mucosal repair of the colon is the focus of the more recent therapeutic medicines. After long-term use, which is necessary for the treatment of IBD, conventional medicines such as aminosalicylates, corticosteroids, immunosuppressants and biological agents have negative effects. As patients become resistant to the therapy and eventually relapse to the active disease state after stopping it, traditional medications are linked to side effects as well as the development of resistance and tolerance [1].

Additionally, colon targeting is challenging due to its distinct location, anatomical changes, and disease states. Rectal formulations are somewhat effective in treating UC; however, they only cover parts of the distal colon. Oral formulations are advantageous in this respect because the typical passage encompasses the entire colon and the entire GIT.

Despite their benefits, oral dose formulations have not been as successful in treating IBD as anticipated because of low stability, first-pass metabolism, acidic and enzymatic degradation, and early systemic absorption from the stomach or small intestine. As a result, the drug's localized concentration in the colon's inflammatory tissues is reduced [1]. Furthermore, common IBD symptoms like excessive diarrhea cause conventional dosage forms like pills, granules, and capsules to be cleared quickly and have a short residence time. Serious side effects result from higher dosages or repeated treatment, which exacerbates the issue.

As a result, the current focus is on developing new drug delivery systems (DDS), such as micro- and nanoparticles, that precisely target and localize the drug to the tissues of the inflammatory colon with better therapeutic efficacy and minimum systemic absorption and side effects [1].

The utilization of naturally derived ingredients or micronutrients and their powerful health effects has been the subject of numerous recent scientific investigations [24]. The natural source, SLM, also known as milk thistle, is an extract from Silybum marianum seeds that contains a combination of flavanolignans with strong intracellular antioxidant properties [25].

For more than 2,000 years, milk thistle has been used as a plant to cure cirrhosis and hepatitis. The flavonolignan combination that makes up milk thistle extract contains roughly 70–80% SLM, which has been demonstrated to have antioxidant action by scavenging ROS and reducing the oxidation of biomolecules [26].

SLM is well-known for its hepatoprotective properties, but in recent years, it has also been shown to help in curing immune-based murine colitis by reducing inflammatory cytokines in the bowel, particularly TNF-α, interleukin-1β (IL-1β), and nuclear factor κB (NF-κB), and mending intestinal histology. Furthermore, it was demonstrated

that in rats given ursodeoxycholic acid and silibinin, the main component of silymarin flavanolignans, there is a relationship between the suppression of NF-κB and a decrease in colitis activity [25].

2.2 Biopharmaceutical Challenges of SLM

Although SLM has several uses, its clinical use for therapeutic benefit is limited by its rapid excretion in urine and bile, poor intestinal absorption, poor water solubility, low oral bioavailability, and increased metabolism. Due to its limited intestinal permeability and low water solubility, SLM is classified as a class IV chemical under the Biopharmaceutics Classification System (BCS). SLM's medicinal effectiveness is limited by its extremely poor water solubility and log P of 1.41 [12]. SLM's poor solubility poses a significant obstacle to its bioavailability because oral administration only results in the observed absorption of 23–47% of the medication [13]. The loading of SLM into a delivery method that could increase its bioavailability is necessary due to these disadvantages. Therefore, SLM formulation options must be carefully considered as silymarin solubilization is crucial to achieving increased bioavailability [12].

Novel techniques are used to create SLM-based formulations with enhanced therapeutic effectiveness. Complexation employing phospholipids or cyclodextrins, microemulsions, nanoemulsions, biocompatible polymer-stabilized solid dispersions, biodegradable polymeric nanoparticles, inorganic nanomaterials, and lipid-based delivery systems are some of the innovative formulation strategies that have been explored [12].

2.3 Advances in Nanoparticulate Drug Delivery

One of the cell-specific targeting techniques, NP-based DDSs, have attracted a lot of attention due to their favorable small size, strong drug loading capacity, and versatile surface shape. Compared to larger submicron particles, smaller NPs (less than 200 nm) have been shown to penetrate the mucus layer more completely and reach the

intestinal tissues. Patients with IBD lose tight junctions and cellular integrity when pro-inflammatory cytokines are activated, and their intestinal permeability often increases. NPs passively direct the medication to the site of inflammation by enhancing their absorption by activated immune cells and utilizing the enhanced permeability effect (EPR). The pharmacokinetics of the encapsulated drug are changed by NP-based delivery in comparison to the free medicament, potentially making it more stable and less immunogenic [3].

Drug solubility can be enhanced by using nano-micelles (NMs), a type of colloidal nanoparticle with a particle size of less than 200 nm. They consist of a blend of amphiphilic block copolymers that can form a supramolecular core/shell structure by self-assembling in an aqueous media. NMs' hydrophobic core serves as a reservoir for the solubilization of medications that are not very soluble. In physiological fluids, the hydrophilic shell stabilizes the core by facing the aqueous environment [27].

Poloxamer (Pluronic) micellar systems have been researched as a way to increase a compound's solubility in aqueous solutions and modify medication release. Because lipophilic substances are integrated into the nucleus with the same feature, the micelles that are created serve as transporters of these compounds in an aqueous medium. The drug shielded against hydrolysis and volatilization in this setting [28]. PLU micelles are essential to nanomedicine as they are efficient nanocarriers for hydrophobic medications, which are difficult to administer because of their low water solubility [29].

The anionic copolymer ES is based on methacrylic acid-methyl methacrylate (1:2) and has a pH-dependent solubility nature. In the stomach and small intestine, where the pH ranges from acidic to neutral, ES shields encapsulated medications from deterioration, resulting in an advance drug delivery system that targets the colon [30].

2.4 PLU as a Drug Carrier

The low CMC values, strong biocompatibility profile and high drug entrapment effectiveness of polymeric surfactants which have a large hydrophobic inner core, make

them a safer and more practical substitute for traditional surfactants. The class that is being studied the most is polyethylene oxide-polypropylene oxide block copolymers, often known as Pluronics or poloxamers [14].

PLU is a kind of poly(ethylene oxide) (PEO)-poly(propylene oxide) (PPO)-poly(ethylene oxide) (PEO) triblock copolymer that is widely used in clinical applications and recognized as an excipient by the British and U.S. Pharmacopoeia [31]. The amphiphilic chemical structure, including a hydrophobic PPO segment and a hydrophilic PEO segment, allows it to incorporate hydrophobic drugs and self-assemble into micelles with a hydrophilic shell and a hydrophobic core in aqueous medium. Poloxamers are members of the triblock copolymer family, which is made up of two hydrophilic lateral sections of polyethylene oxide (PEO) and a hydrophobic central component of polypropylene oxide (PPO). Their ability to self-organize into micelles is contingent upon the PEO/PPO ratio, which typically ranges from 10 to 200 nm [28] The core of micelle is composed of PPO while the surrounding shell is the hydrophilic PEO. Poloxamer's hydrophobic portion can be used to implant hydrophobic drugs. Micelle characteristics, including form, aggregation, critical micelle temperature (CMT) and CMC, are determined by the molecular weight of the segments. Due to an increase in the system's hydrophobicity, the CMC value dropped as the PPO concentration rose. The CMC values also showed a direct correlation with the PEO content. Further micelle destabilization was caused by higher PEO concentrations [32].

2.5 Role of ES In Colon Targeted Drug Delivery

The creation of pH-sensitive micro and nanoparticles makes colon targeting easier and gets beyond the limitations of basic micro and nanoparticles [1]. The pH-sensitive method also makes it easier to adopt herbal treatments, which have a number of medicinal benefits but have pharmacokinetic problems [33]. The anionic copolymer polymethylmethacrylate ES is based on methacrylic acid-methyl methacrylate (1:2) and has a pH-dependent solubility nature. ES creates a colon-targeted drug delivery system by shielding encapsulated medications from deterioration in the stomach and small intestine, where the pH ranges from acidic to neutral [30].

2.6 SLM Formulation Studies

TABLE 2.1: Summary of SLM Formulation Studies in the Last Decade.

Formulation Type	**Objective**	**Key Findings**
PVP-PEG polymeric composite (solid dispersions)	To enhance water solubility, improve oral bioavailability dissolution rate.	Remarkable drug solubility in water and enhanced dissolution. Solubility found 1150 times greater compared to SLM alone [34].
Phytosome	To enhance oral bioavailability with improved safety and stability.	Improved drug loading and entrapment efficiency; formulation exhibited enhanced stability [35].
Lyophilized nanosuspension tablets (LNTs)	To improve solubility; enhances dissolution rate and bioavailability.	Efficient disintegration time (<30s) and decreased friability (<1%) [36].
Chitosan-functionalized lipid-polymer hybrid nanoparticles (CS-LPNs)	To enhance oral delivery and to treat non-alcoholic fatty liver.	Substantial reduction in in-vitro lipid deposition assay and TG levels; 14.36-fold increase in oral bioavailability in rats; reduced macrovesicular steatosis [37].
Solid dispersions (SD)	To improve dissolution rate, enhance bioavailability and oral absorption.	Improved biopharmaceutical activities [38].
Nanostructured lipid carriers (NLCs)	To enhance drug entrapment efficiency and treat liver and lymphatic disorder.	Improved drug entrapment efficiency; in-vivo studies showed liver uptake via lymphatic pathway [39].
Mesoporous silica nanoparticles (MSNs)	To enhance bioavailability and hepatoprotective activities.	Oral SLM MSNs superior to SLM alone in liver function parameters and dissolution [40].
Nano emulsions	To enhance oral bioavailability and antioxidant activity.	Improved oral bioavailability and antioxidant activity compared to free drug [41].
Nanoemulsions	To improve oral bioavailability, solubility, and therapeutic efficacy.	Enhanced solubility and substantial increase in permeability [42].
Super saturable self-nano emulsifying drug delivery system (S-SNEDDS)	To improve bioavailability, therapeutic outcomes (hepatoprotection), and inhibit drug precipitation.	Compared favorably to branded Legalon®; combining SNEDDS with PLU enhanced bioavailability and hepatoprotective effects [43].

Table 2.1 continued from previous page

Formulation Type	**Objective**	**Key Findings**
Pluronic nano micelles	To enhance aqueous solubility, bioavailability, drug transport, and cancer cellular uptake.	Improved anticancer activity with increased aqueous solubility, bioavailability, and drug transport [44].

Chapter 3

Materials and Method

3.1 Materials and Equipment

Silymarin (SLM) generously provided by Amson Vaccines & Pharma, Islamabad. Polymethylmethacrylate Eudragit® S100 (ES) sourced from Evonik® Germany. Pluronic F127 (Poloxamer 407) (PLU) sourced from Sigma-Aldrich (CHEMEI GmbH Germany). Methanol acquired from Duksan Chemicals, Korea. Sodium hydroxide (NaOH) Sigma-Aldrich (CHEMEI GmbH Germany). Fresh distilled water used in the formulation was prepared in the research laboratory at Faculty of Pharmacy, Capital University of Science and Technology, Islamabad. Dextran sodium sulfate (DSS) was proCured from Macklin BioChemical Co., Ltd. (CH1002, China). Equipment used for formulation development are; digital weighing balance, Magnetic stirrer, sonicator, homogenizer, lyophilizer utilized for freeze drying, stability chambers were used for stability studies. Centrifuge was used during encapsulation efficiency determination process. UV spectrophotometer for absorbance, X-ray diffractometer, stalagmometer for CMC determination, Zeta sizer for particle size determination.

3.2 Method

3.2.1 UV-Visible Calibration Curve Method

The UV-visible spectrophotometer was used to determine the SLM calibration curve at 288 nm. First, a stock solution was made by dissolving 100 mg of SLM in a 100 mL volumetric flask, adding 20 mL of methanol first, and then adding enough (q.s) to reach a final volume of 100 mL, 0.5 mL, 1.0 mL, 1.5 mL, 2.0 mL, and 2.5 mL were taken from the stock solution and placed in different volumetric flasks to create various dilutions of 5 μg/mL, 10 μg/mL, 15 μg/mL, 20 μg/mL, and 25 μg/mL.

3.2.2 Estimation of Critical Micelle Concentration

The Critical Micelle Concentration (CMC) of the PLU copolymer forming the micelles was determined by the surface tension measurement method at 25^{o}C. For this method, different concentrations of water-soluble PLU (1%w/v to 8%w/v) were formulated. The mass of each concentration of polymer solutions and water corresponding to 50 drops was identified by using stalagmometer. Using the found mass values and the surface tension of the water, the surface tension of PLU was calculated according to the Hagen-Poiseuille equation;

$$\gamma sample/\gamma water = msample/mwater$$

In this equation, γsample (N/m) represents surface tension of the copolymer solution, γwater (N/m) is 0.073 (at 25^{o}C), msample (g) represents the mass of the copolymer solution, mwater (g). CMC was determined by drawing a concentration graph against the calculated surface tension [45].

3.2.3 Preparation of Pluronic micelles

Pluronic micelles were prepared by the dissolution method with the control of critical parameters. Initially, 7.0 % w/v (350 mg) PLU was added in 5 mL distilled water

and continuously stirred at 1000 rpm at 25^{o}C for an hour [46].

3.2.4 Drug Loading in Pluronic micelles

SLM 10 mg was added in methanol (2 mL) and sonicated until it was completely dissolved. Then the drug was added in the aqueous solution of PLU dropwise using a 22G needle syringe with continuous stirring on a magnetic stirrer at 25^{o}C for 30 minutes [46].

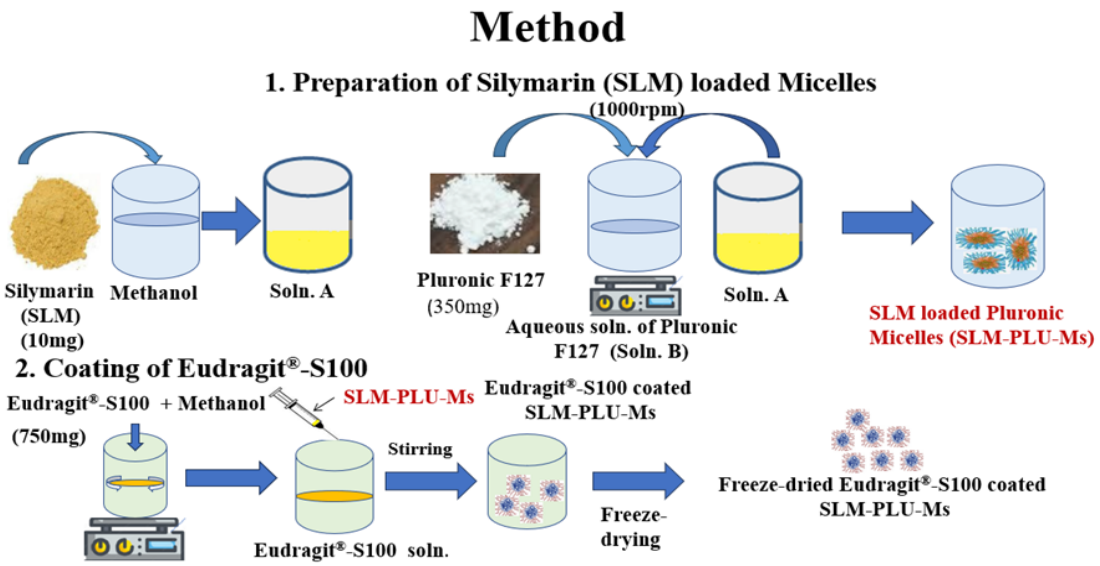

FIGURE 3.1: SLM-Plu-Ms preparation scheme.

3.2.5 Coating of Pluronic micelles with ES

700 mg of ES was added to 8 mL of methanol and 1 mL of 0.1 N NaOH and sonicated until it was completely dissolved. Pluronic micelles were coated with ES by adding ES solution in the micellar solution dropwise using a 22G needle and homogenized at 2000 rpm by using an overhead homogenizer for 9 minutes. The formulation was kept at continuous stirring at 1000 rpm for 12 hours to remove organic solvent [27].

3.2.6 Lyophilization of SLM-ES-PLU-Ms

The prepared formulation was frozen at -20^{o}C for 8 hours before lyophilization in a freeze dryer. The lyophilization protocol consisted of primary drying at -40^{o}C and

0.1 mbar for 12 hours, followed by secondary drying at 25^{o}C and 0.01 mbar for an additional 12 hours.

3.3 Optimization of Formulation

To ensure the optimal quality of polymeric micelles, the formulation conditions and parameters were optimized by using Design Expert® software. Design Expert® facilitated the formulation development with desired outcomes [47].

Box-Behnken design was considered because it offers fewer experimental runs, mitigates extreme combinations, is easy to interpret, and reduces cost and time [48].

After initial preliminary studies, polymer concentration (A), stirring speed (B) and homogenization time (C) were selected to be the most influential independent variables affecting product outcomes.

The 3^3 Box-Behnken design, a response surface model, was chosen to design experimental conditions based on these variables and their corresponding effects. It generated 17 different combinations of independent variables and their effect on response variables particle size (Y_1), zeta potential (Y_2), and polydispersity index (Y_3) [49].

3.4 Physiochemical Characterization

3.4.1 Determination of Particle Size, Zeta Potential and Polydispersity Index

The dynamic light scattering (DLS) technique was used to determine the particle size, zeta potential, and polydispersity index (PDI) of SLM-ES-PLU-Ms and uncoated micelles SLM-PLU using a Zeta sizer 2000 HS (Malvern Instrument, Malvern, UK) at 37 $\pm$ 0.1^{o}C [19].

3.4.2 Determination of Encapsulation Efficiency and Drug Loading

The indirect method was used to estimate the SLM-ES-PLU-Ms' encapsulation efficiency. After centrifuging SLM-ES-PLU-Ms at 13500 rpm for 30 minutes at 25 ^{o}C, the free drug was collected in the form of a clear supernatant and examined at 288 nm using a UV-visible spectrophotometer as part of the indirect method. The amount of drug that was free was calculated using a standard calibration curve. The percent encapsulation efficiency and drug loading were calculated by the following formula [50, 51].

$$\% \, EE = \frac{Total \; Drug - Free \; Drug}{Total \; drug} \times 100 \tag{3.1}$$

$$DL\% = \frac{Weight \; of \; SLM \; in \; Micelles}{Total \; Micelles \; Weight \; (SLM \; + \; PLU)} \times 100 \tag{3.2}$$

3.4.3 Morphological Analysis

Scanning Electron Microscopy (SEM) was used to analyze the formulation morphology. A SEM template was coated with a few drops of the micellar formulation, which was subsequently dried. After applying a 5 nm layer of gold to the samples, SEM (JEOL, JSM–IT 100) measurements were carried out using electron beams with a 5 kV accelerating potential. The photos were processed with SEM/JSM 5000 software [52].

3.4.4 Attenuated Total Reflectance - Fourier Transform Infrared Spectroscopy

An attenuated total reflectance - fourier transform infrared spectroscopy (ATR-FTIR) spectrometer (Bruker® Alpha GmbH, Germany) was used to record the ATR-FTIR spectra. For every sample, a spectrum scan was performed in the wave number range of 4500 cm^{-1} to 1000 cm^{-1}. Any potential interactions between SLM, excipients, and the micelles were examined using this technique [53].

3.4.5 X-ray Powder Diffraction Analysis

The nature of the drug within the micelles was determined by X-Ray powder diffraction (XPRD) analysis of the drug and drug-loaded carriers. A Bruker® AXS GmbH, Germany, X-ray powder diffractometer was used for the analysis [11].

3.4.6 Drug Release Studies and Kinetics

Drug release studies were performed in simulated gastric fluid (SGF) at pH 1.2 and simulated intestinal fluid (SIF) at a pH of 7.4 from nanocarriers using dialysis membrane method [11]. The drug release kinetics and mechanism of drug release from the prepared formulation were determined by mathematical kinetic models using DD solver program [50].

3.4.7 Stability Studies

The stability of SLM-loaded polymeric micelles was evaluated according to ICH guidelines for storage under accelerated conditions ($25^oC \pm 2^oC$ and $60 \pm 5\%$ relative humidity; RH), compared with long-term conditions in a refrigerator ($5^oC \pm 3^oC$) for 30 days [19].

3.5 In Vivo studies

3.5.1 Ethical Statement

In vivo study was carried out in accordance with institutional and national guidelines for the humane treatment and use of lab animals. The Capital University of Science and Technology, Islamabad's Research and Ethical Committee (REC) examined and approved the study protocol (REC/FoP/F2024/12). The experimental procedures adhered to globally accepted standards. Male BALB/c mice used in this study were

treated, housed, and handled with care as per the protocols by the US-based Association for Assessment and Accreditation of Laboratory Animal Care International (AAALAC).

3.5.2 Experimental Animals

The male BALB/c mice used in this study were 3–4 weeks old and weighed between 29 and 30 grams. The mice were housed in normal humidity and temperature conditions for a week to acclimate them. The animals were given unlimited access to food and water while being kept in sterile, standard laboratory conditions.

3.5.3 Randomization of Animals in Groups

The animals were split into four groups (n=5) at random: the normal control group, the group that received free drug solution, the group that received drug-loaded micelles, and the negative control group that received drinking water and DSS.

Table 3.1: Experimental Groups and Treatment

Group No.	**Group Type**	**Dose and Route of Administration**
Group 1	Normal Control Group	Simple drinking water and food
Group 2	Negative Control Group	3% w/v DSS through the Oral route
Group 3	Free Drug Receiving Group	5 mg/kg SLM through the Oral route
Group 4	Treatment Receiving Group	SLM-ES-PLU-Ms (dose eq. to 5 mg/kg) Oral route

3.5.4 Colitis Induction and Measurement of Therapeutic Indices

Three percent w/v DSS was added to the water for seven days in order to cause experimental colitis in the BALB/c mice. Experimental intestinal inflammation was induced by following the described protocol [50]. The first group was maintained as a standard control group, and during the experiment, they were given standard drinking water. Following seven days of receiving drinking water containing DSS, the

second group—a negative control, or diseased group—was left untreated with distilled water alone. Following a seven-day induction period with DSS-drinking water, the third and fourth groups administered oral gavages of free drug solution (SLM) and SLM-ES-PU-Ms, respectively. From days 7 to 14, every treated group was given an identical oral dose of SLM once daily (dose = 5 mg/kg), either as micelles or as free medication. The liquid formulation (300 μL) was administered based on body weight. Daily calculations of the disease activity index (DAI) were used to gauge the severity of colitis. DAI, which is a composite score of bleeding, stool consistency (0, normal; 1, soft; 2, very soft/pasty; 4, diarrhea), and bodyweight loss (1, 1–5 percent; 2, 5–10 percent; 3, 10–20 percent; 4, >20 percent), was computed. Colon sections from cecum to anus were removed at the conclusion of the experiment. A few metrics, such as colon length and the wet colon weight to length ratio, were assessed as indicators of inflammation [50].

TABLE 3.2: Weight loss score %

Weight Loss (Score)	**% Loss**
0	0%
1	1–5%
2	5–10%
3	10–20%
4	>20%

TABLE 3.3: Stool consistency score

Score	**Stool Consistency**
0	Well-formed pellets
1	Soft but still formed
2	Very soft, pasty, semi-formed
4	Diarrhea / liquid stool
4	>20%

TABLE 3.4: Bleeding score

Score	**Bleeding**
0	Negative hemoccult
1	Positive hemoccult
2	Blood traces visible
4	Gross rectal bleeding

TABLE 3.5: Distress scoring

Symptoms	**0**	**1**	**2**	**3**
Dulled Ruffled Coat	Shiny coat	Coat raised around neck only	Coat raised around neck and belly	Coat raised entire animal
Change in temperament	Normal disposition	Agitated	Stress marks on eyes, nose and paws	Stress marks with hunching
Reluctance to move up	Movement as lift the lid	Movement once hand place near mice	Movement only after picking up mice	No movement while handling

3.5.5 Histological Analysis of Colon

All four groups were then excised colon tissues that were segmented in smaller length, fixed in buffered 10% formalin, embedded in paraffin, sliced 5 μm thick with a microtome, stained with hematoxylin and eosin or periodic acid Schiff. Samples were observed microscopically and graded on a scale from 0 to 5 on the basis of inflammation severity [50].

TABLE 3.6: Histological scoring

Histological Parameters	**Description**	**Score**	
Mucosa	Epithelial cell	Prolong epithelial cell and crypt	1
		Destruction of barrier	2
		Ulcer (30% <loss <60%)	3
		Ulcer (loss >60%)	4
	Immune cell	Mild infiltration	1
		Moderate infiltration	2
		Severe infiltration	3
Sub-mucosa	Immune cell	Mild infiltration	1
		Moderate infiltration	2
		Severe infiltration	3

3.6 Statistical Analysis

The statistical analysis was performed using MS Excel, GraphPad Prism. All values are represented as mean ± standard deviation (SD). The level of significance was considered 0.05* ($\alpha = 0.05$), 0.01** ($\alpha = 0.01$) and 0.001*** ($\alpha = 0.001$) using the one-way analysis of variance (ANOVA).

Chapter 4

Results

4.1 Pre-formulation Studies

4.1.1 UV-Visible Calibration Curve

A calibration curve for silymarin was constructed at a wavelength of 288nm. This curve is critical in quantifying silymarin concentrations in solution via UV-Visible spectrophotometry and ensuring accuracy in subsequent formulation. The calibration curve of silymarin showed a precise and accurate linear graph plotting absorbance vs concentration (μg/mL). It was used to establish a quantitative analytical method using UV-Visible spectrophotometry. The linear equation; y = 0.0359x + 0.009 indicates consistent rise in absorbance as the concentration of silymarin is increased, the slope reflects the method's sensitivity to concentration changes.

Table 4.1: Concentration Vs Absorbance

Concentration (μg/ml)	**Absorbance**
5	0.189
10	0.336
15	0.551
20	0.722
25	0.908

R^2 = 0.9999 indicates significant linearity and high method reliability across the 5 -25μg/ml. This near-perfect R^2 confirms minimal deviation of experimental data from the regression line.

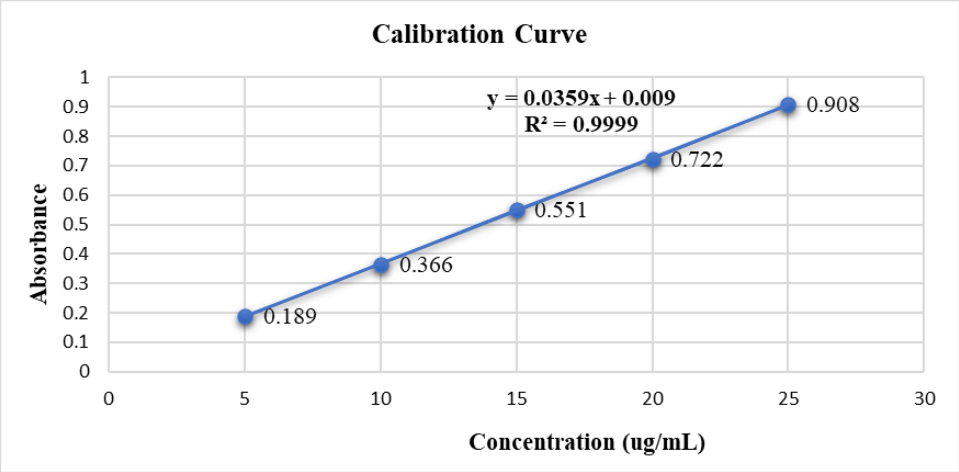

FIGURE 4.1: Calibration Curve

4.1.2 Critical Micelles Concentration of Pluronic Micelles

CMC is a key factor that defines the stability and effectiveness of formed micelles. PLU CMC value, micellization behaviour, and self-assembly thermodynamics in aqueous systems are all significantly impacted by its hydrophilic-lipophilic balance (HLB). Its molecular structure, which consists of hydrophilic PEO blocks and a hydrophobic PPO core, results in a notably high HLB value is 22.

The CMC is the lowest concentration of Pluronic polymer for which self-assembly of unimers into micelles occurs, and this value largely affects drug encapsulation properties and system stability. The CMC of Pluronic micelles was established by the surface tension method according to the reported method [45]. The CMC of the PLU copolymer in the formation of micelles was measured by the surface tension method at 25^{o}C. For this method, eight different concentrations of water-soluble PLU polymer were prepared. With the help of a stalagmometer, the mass of each concentration of polymer solutions and water corresponding to 50 drops was found. By using the found mass values and the surface tension of the water, the surface tension of PLU is calculated according to the Hagen-Poiseuille equation [45].

TABLE 4.2: Pluronic F127 Concentration and Surface Tension

Pluronic F127 Concentration (%)	**Surface Tension**
1%	0.075
2%	0.076
3%	0.075
4%	0.077
5%	0.074
6%	0.074
7%	0.074
8%	0.074

The surface tensions for aqueous solutions of PLU measured at different concentrations (1-8%) exhibited typical behavior indicative of micellization: surface tension values fluctuated slightly from 0.074 to 0.077, with a peak value observed at 4% concentration (0.077), after which the surface tension plateaued at 0.074, indicating saturation of surface-active sites and formation of micelles; this confirms that further increases in concentration do not significantly decrease surface tension above CMC. The graph for concentration of Pluronic (%) vs surface tension is constructed, showing that the CMC of PLU micelles is 5%w/v at 25^{o}C.

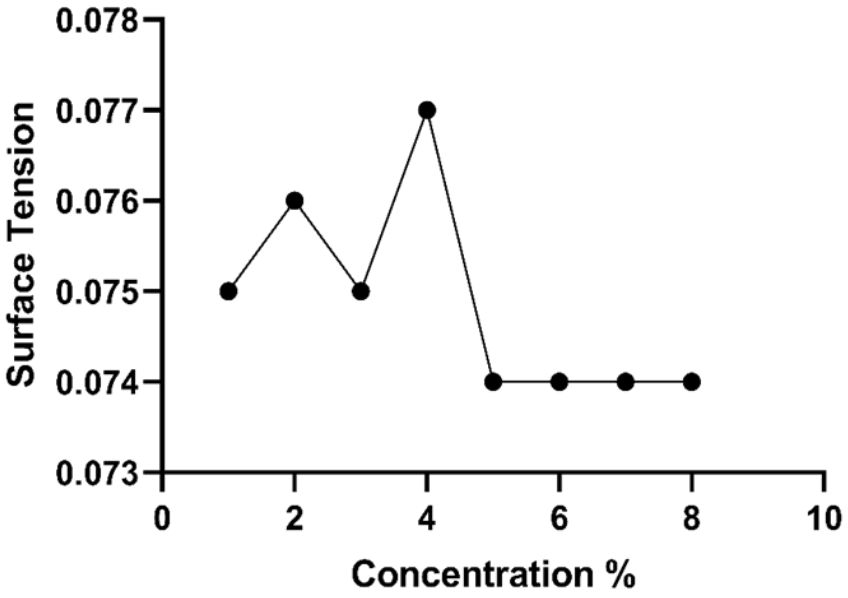

FIGURE 4.2: Critical Micelles Concentration (Concentration Vs Surface Tension Graph)

After micellization, PLU amphiphilic structure encourages the formation of spherical micelles with a hydrated PEO corona encasing a hydrophobic PPO core. These micelles can be used effectively to solubilize hydrophobic molecules and regulate release kinetics in pharmaceutical and biomedical systems because of their high HLB value, which also makes them more sterically stable, biocompatible, and aqueously soluble.

ES dual hydrophobic and hydrogen bonding interactions alter the CMC in PLU micellar systems. ES unionized carboxyl groups at neutral or acidic pH interact associatively with the PEO-PPO-PEO structure of PLU to improve micelle stability and reduce the CMC. The polymer is soluble upon ionization at intestinal pH, which results in controlled micellar disassembly and elevated CMC, supporting colon-targeted release mechanisms.

4.2 Optimization of SLM-ES-PLU-Ms

The present study utilized a three-level, three-factor Box-Behnken Design (BBD) to statistically optimize the formulation (SLM-ES-PLU-Ms).

The goal was to understand the effect and variations of independent variables polymer concentration (A), stirring speed (B) and homogenization time (C) onto the micellar formulation dependent variables like particle size (Y_1), zeta potential (Y_2) and polydispersity index (Y_3) which directly impact formulation stability, drug release, and bioavailability.

Design Expert® software was used to construct the experimental design matrix, perform regression analysis, and interpret the response surface models.

4.2.1 Experimental Design Overview

A total of 17 experimental runs were performed. BBD was employed using Design Expert® software to statistically evaluate the effect of three independent variables on three dependent variables.

Std	Run	Factor 1 A: Polymer conc. mg	Factor 2 B: Stirring speed rpm	Factor 3 C: Homogenization time minutes	Response 1 Particle size nm	Response 2 Z-potential mV	Response 3 PDI
7	1	175	1000	9	494.4	-11	0.513
14	2	437.5	1000	6	314.1	-14.75	0.626
1	3	175	500	6	1907	-9.38	0.411
6	4	700	1000	3	66.21	-20.05	0.412
10	5	437.5	1500	3	377.1	-2.06	0.858
8	6	700	1000	9	42.80	-42	0.182
3	7	175	1500	6	198.9	-40.4	0.981
11	8	437.5	500	9	56.6	-41.55	0.669
4	9	700	1500	6	41.05	-44.88	0.427
9	10	437.5	500	3	83.91	-14.05	0.644
5	11	175	1000	3	216.25	-46.8	0.614
13	12	437.5	1000	6	314.1	-14.75	0.626
15	13	437.5	1000	6	314.1	-14.75	0.626
2	14	700	500	6	38.23	3.5	0.351
17	15	437.5	1000	6	314.1	-14.75	0.626
16	16	437.5	1000	6	314.1	-14.75	0.626
12	17	437.5	1500	9	89.16	-51.7	0.332

FIGURE 4.3: Experimental Runs by Design Expert®

p-value shading: **p < 0.05** 0.05 ≤ p < 0.1 p ≥ 0.1

	Intercept	A	B	C	AB	AC	BC	A^2	B^2	C^2
Particle size	304.909	**-328.365**	-172.441	-7.39625	**427.73**	-75.055	-65.1575			
p-values		**0.0221**	0.1857	0.9526	**0.0318**	0.6711	0.7121			
Z-potential	-23.2688	0.3375	-9.695	-8.0925	-4.34	**-14.8**	-5.535			
p-values		0.9529	0.1123	0.1768	0.5937	**0.0897**	0.4982			
PDI	0.626	**-0.143625**	0.065375	**-0.10425**	-0.1235	-0.03275	**-0.13775**	**-0.13975**	0.05625	-0.0565
p-values		**0.0064**	0.1237	**0.0269**	0.0521	0.5551	**0.0351**	**0.0301**	0.3111	0.3091

FIGURE 4.4: Coefficient data by Design Expert®

4.2.2 Analysis of Particle Size

The range of particle size for the 17 formulations was found between 41.05 nm and 1907 nm, demonstrating significant responsiveness to changes in the input parameters. The maximum particle size of 1907 nm recorded in Run 3 was associated with a polymer concentration of 175 mg, stirring speed of 500 rpm, and moderate homogenization time of 6 min, suggesting weak micelle formation and coalescence resulting from low energy input and stabilizer below critical availability. On the other hand, run 9 produced the minimum particle size of 41.05 nm with 700 mg of polymer, 1500 rpm stirring speed, and 6 min homogenization time. This indicates that sufficient shear force coupled with surfactant micelle coating, accomplished via stirring, allowed droplet breakup

and micelle formation.

The second order polynomial Eq. (4.1) for establishing an empiric relationship between particle size (Y1) and independent variables is;

$$Y_1 = 304.91 - 328.36A - 172.44B - 7.04C + 427.73AB - 75.05AC - 65.16BC \quad (4.1)$$

The equation illustrates the multi-variable influence on particle size, where a positive sign indicates a synergistic effect and a negative sign shows an antagonistic effect.

Among the linear terms, polymer concentration had the strongest negative contribution, implying that increasing its level substantially reduced particle size. Similarly, stirring speed also demonstrated a pronounced negative effect, while homogenization time exerted only a minor influence on the reduction of size.

4.2.2.1 Independent Variables effect on Particle Size

4.2.2.1.1 Polymer concentration The increase in ES concentration from 175 mg to 700 mg led to a decrease in particle size, resulting from improved surface stabilization and reduction of viscosity damping. However, that increase in viscosity at some point beyond 700 mg resulting in Run 2 particles getting larger suggests an inefficient dispersion system dominated resulting in stabilizing surfactant capped polymers.

4.2.2.1.2 Stirring Speed A noticeable increased in particle size was observed with stirring speed above 500 and up to 1500 with moderate polymer concentrations, indicated a significant correlation between micelle formation and surfactant concentration under considerable shear forces.

4.2.2.1.3 Homogenization Time The consequences of longer homogenization (e.g., 9 min) were inconsistent. System saturation or reaggregation effects might explain why excessive time did not lead to further particle size reduction for some

cases, although certain cases like Run 6 (700 mg, 1000 rpm, 9 min) yielded small particles (42.80 nm).

4.2.3 Analysis of Zeta Potential

The zeta potential varied between the values of -51.7 mV (Run 17), to +3.5 mV (Run 14) with most values in the strongly negative section, thus the system is very well electrostatically stabilized. More negative zeta potentials (full negative potential, i.e., -44.8 to -51.7 mV) were measured at a higher concentration of the polymer and/or higher stirring velocities. Values of low or positive zeta potential (lowest data corresponded with +3.5 mV, in Run 14) indicated either overloading of polymer or micelle saturation that did not allow surface ionization and full polymerization with 700 mg polymer.

The multivariate regression Eq. (4.2) for zeta potential and its relationship with independent variables is;

$$Y_2 = -23.27 + 0.3375A - 9.70B - 8.09C - 4.34AB - 14.80AC - 5.54BC \quad (4.2)$$

The model suggests that polymer concentration (A) exerted a minimal positive effect (+0.3375), while both stirring speed (B) and homogenization time (C) had strong negative effects (-9.70 and -8.09, respectively), shifting the zeta potential toward more negative values.

4.2.3.1 Independent variables effect on Zeta Potential

4.2.3.1.1 Polymer Concentration The intermediary concentration of 437.5 mg seemed to have the most beneficial results since it delivered a noticeably adverse zeta potential (-51.7 mV), which represents an uncovered surface charge presumably constricted by the protective coating.

4.2.3.1.2 Homogenization Time The time of homogenization indicating that there is a possibility of polymer overloading or saturation of micelles that did not

allow a complete surface coverage, of the ES polymer, ionization. More negative zeta potential (∼ -51.7 mV) was observed with moderate concentrations (437.5 mg) that presumably suggested optimal coating and exposure of surface charges.

4.2.3.1.3 Stirring Speed Based on experimental results, high stirring rate directly relates with a rise in the zeta potential magnitude.

The latter effect may be seen in a systematic juxtaposition of two consecutive runs: Run 2 (500 rpm, -9.38 mV) and 17 (1500 rpm, -51.7 mV).

4.2.4 Analysis of PDI

The PDI values were between 0.18 and 0.991 indicating that there was a great difference in the uniformity of micelles.

Run 6 possessed the lowest PDI (0.18) which indicated that a very homogenous micellar population was obtained (preparation conditions were 700 mg polymer concentration, stirring speed 1000 revolutions per minute (rpm) and the homogenization time was 9 min).

In contrast, run 7 (175 mg, 1500 rpm, 6 min) exhibited the greatest PDI (0.991) which means that there is co-existence of heterogeneous micellar populations or structurally unstable.

3^3 Box-Behnken model provides Eq. (4.3) describing influence of independent variables on PDI;

$$\begin{aligned} Y^3 = {} & 0.0620 - 0.1436A - 0.0654B - 0.1042C - 0.1235AB - 0.0328AC \\ & - 0.1378BC - 0.1398A^2 + 0.0563B^2 - 0.0565C^2 \end{aligned} \tag{4.3}$$

The linear terms revealed that all three independent variables had a negative effect on PDI, with polymer concentration (A) (-0.1436) exerting the strongest influence, followed by stirring speed (B) (-0.0654) and homogenization time (C) (-0.1042).

This suggests that increasing polymer concentration and homogenization time within the experimental range markedly improved micellar uniformity, while stirring speed contributed to a lesser but still beneficial reduction in PDI.

4.2.4.1 Independent Variables Effects on PDI

4.2.4.1.1 Polymer concentration Intermediate addition and double ratio of polymer to surfactant 2:1 generated very homogeneous micelle populations, with maximum distribution index value of 0.332-0.626 and similar ratios of surfactant to cores within the preparations. These results indicate that moderate loading can be an ideal approach to the formation of uniform and steady-state micelles and enable achieving reproducibility between batches.

4.2.4.1.2 Stirring speed According to observational data, the PDI values decrease with increasing speed. This trend can be explained by the fact that the energy distribution becomes more uniform as speed increases.

4.2.4.1.3 Homogenization time Wider variation in PDI was observed for extremely short (3 min) or long (9 min) times, indicating that an intermediate range (∼6 min) is ideal for preserving a uniform size distribution.

4.2.5 Combined Response Analysis and Optimization

4.2.5.1 Best Performing Formulation

The observed data indicated that Run 6 had a small particle size, a high negative zeta potential, and a low PDI, concentration of ES polymer is 700 mg. The speed of stirring is 1000 rpm. Homogenization takes nine minutes resulting in Zeta potential of of -42 mV, particle size of 42.80 nm, and PDI of 0.182.

4.2.5.2 Formulation With the Worst Performance

Run 3 had the highest particle size, lowest negative zeta potential, and the highest PDI. The concentration of polymer: 175 mg, stirring speed: 500 rpm and homogenization time: 6 minutes resulting in Zeta potential of -9.38 mV, particle size of 1907 nm, PDI of 0.411 These results illustrate the effect of stirring speed and concentration of polymer on micellar properties.

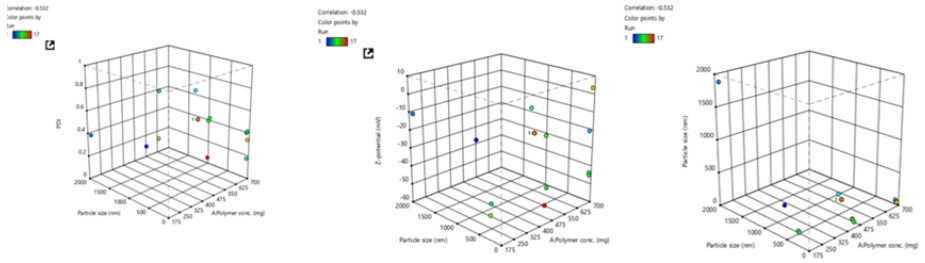

FIGURE 4.5: Surface response plot showing effect of polymer concentration on PDI, Z-potential and particle size.

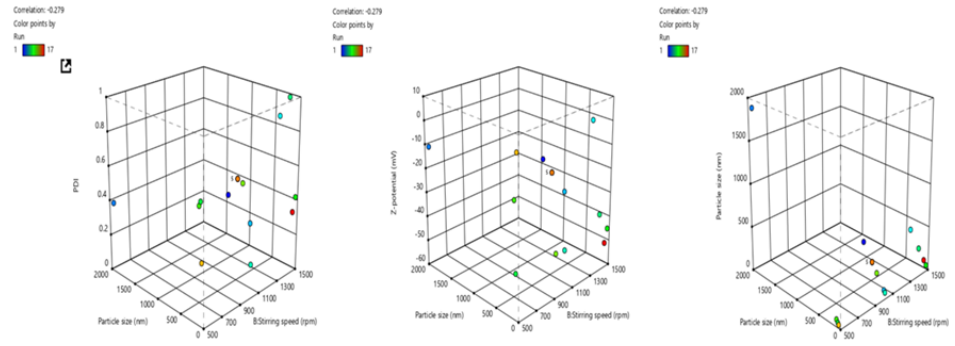

FIGURE 4.6: Surface response plot showing effect of stirring speed on PDI, Z-potential and particle size.

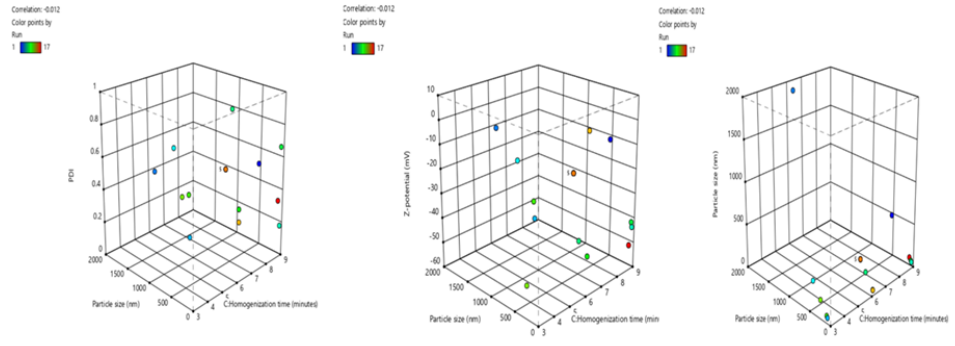

FIGURE 4.7: Surface response plot showing effect of homogenization time on PDI, Z-potential and particle size.

4.3 Particle Size (z), PDI, and Zeta Potential

The physicochemical properties of micelles are crucial for the efficacy, stability, and specificity of pH-responsive drug delivery systems, especially in pathological environments such as inflamed tissues. The biodistribution, cellular uptake, and accumulation in tumors or inflammation is critically affected by the size of the micelle, while zeta potential affects the cellular uptake, circulation time, and aggregation behavior. In this study, the optimized formulation (F6) was evaluated using dynamic light scattering (DLS) measurements that indicated a Z-average particle size 42.80 nm with a peak at 51.10 nm. A value of 42.8 nm implies that the micelles are in optimal size range (10-200 nm) for EPR effect for passive targeting. The low PDI 0.182 indicates good size distribution, which also suggests a stable F6 micelle formulation well suited for targeted, pH-responsive drug delivery.

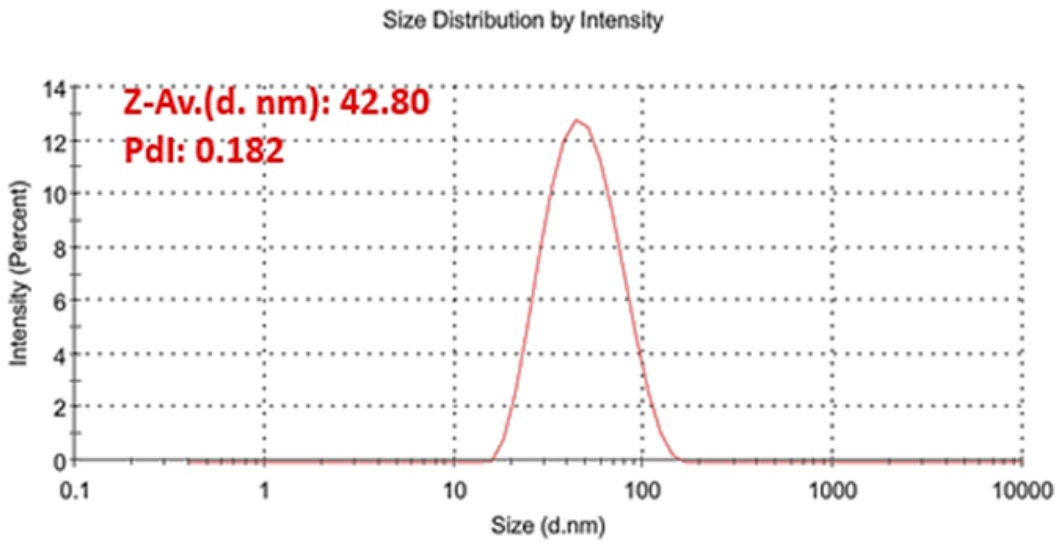

FIGURE 4.8: Size & PDI of SLM-ES-PLU-Ms

The zeta potential of micellar formulation, was found -42.0 mV, suggesting excellent colloidal stability as particles with zeta potentials greater than ±30 mV typically resist aggregation because of strong electrostatic repulsion; surface charge is negative and probably arises from the presence on the micelle surface of ES, an anionic copolymer that will increase surface charge density and physical stability of the formulation. The single sharp peak in the distribution indicates uniform surface potential throughout

the formulation, while conductivity of 0.0451 mS/cm indicate a low ionic strength environment with little interference to the zeta potential measurement; finally, the high negative zeta potential further demonstrates that micelles are electrostatically stable which is desirable for shelf-life and drug delivery performance.

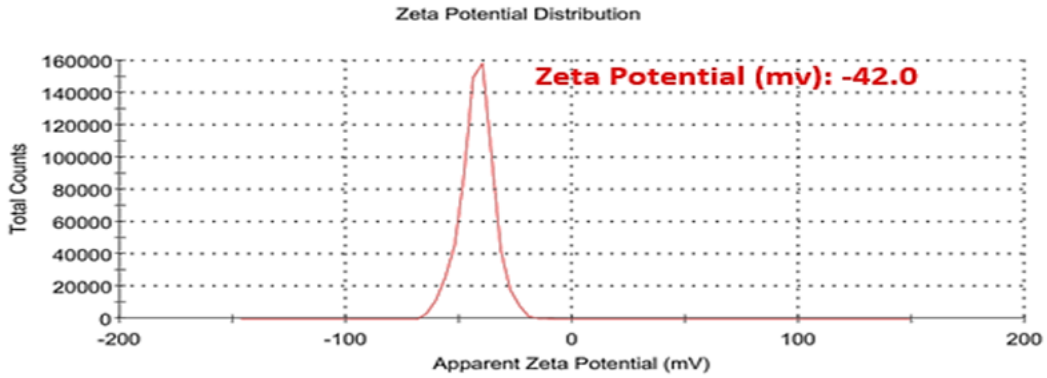

FIGURE 4.9: Zeta Potential SLM-ES-PLU-Ms

4.4 Encapsulation Efficiency

The percentage EE of SLM-ES-PLU-Ms was 79.63%, which confirmed successful drug entrapment in the polymeric micellar system. The EE of SLM-PLU micelles was 72.26% while the SLM-ES-PLU-Ms exhibited a higher EE. This increase in EE upon ES coating can be attributed to the secondary polymeric barrier, which likely decreased drug diffusion from the micellar core during formulation and storage. The polymer PLU alone forms micelles with hydrophobic PPO cores and hydrophilic PEO shells, solubilizing hydrophobic drugs such as SLM. However, the incorporation of a steric and pH-responsive shield around the micellar surface by addition of ES, particularly under neutral and basic conditions where ES is intact, likely enhanced drug retention. The ES layer also prevents destabilization or premature drug leakage in aqueous environments and improves formulation stability. In addition, the coating enhances the possibility for targeted intestinal delivery since ES dissolves at pH $>$ 7 while protecting the drug throughout the gastric environment. In general, these results demonstrated that ES could stabilize the micellar system and increase the drug entrapment, thus confirming its potential as a strategy to improve oral delivery of poorly water-soluble drugs such as SLM.

TABLE 4.3: Physicochemical characteristics of SLM-PLU-Ms and SLM-ES-PLU-Ms

Formulation	**EE%**	**DL% (μg/mg)**	**% Yield**
SLM-PLU-Ms	72.26 ± 0.15	69.14 ± 0.34	33.16 ± 0.18
SLM-ES-PLU-Ms	79.63 ± 0.11	61.30 ± 0.08	35.92 ± 0.16

4.5 Morphological Analysis Scanning Electron Microscopy

Scanning Electron Microscopy (SEM) was used to examine the surface morphology and topographical features of the micelles, as shown in Figures, showing important microstructural features related to the micelle, SEM image shows a relatively smooth and uniform film surface with some spherical and semi-spherical domains.

The central region is characterized by a deep crater-like depression surrounded by fine crack networks that may originate from localized micellar aggregation or collapse during vacuum drying, and radial cracks suggesting mechanical stress induced by solvent evaporation or surfactant packing behavior. These observations are complemented with additional detail at the nanoscale as seen in Figure 4.10 which shows wrinkled textures and interconnected valleys typical of dehydrated micellar films.

The lack of crystalline facets indicates an amorphous morphology, consistent with the self-assembled nature of micelles stabilized by amphiphilic surfactants. Furthermore, there is no discernible phase separation or particle detachment, signifying good surface adhesion and cohesive aggregation, while these images corroborate the formation of micellar aggregates.

The homogeneous dispersion, absence of crystalline ordering, and occasional flattening effects are consistent with dried micellar systems, and they are in agreement with results from dynamic light scattering (DLS) and zeta potential measurements, which indicate that nano-sized electrostatically stable micelles would form, tending to aggregate softly under drying conditions.

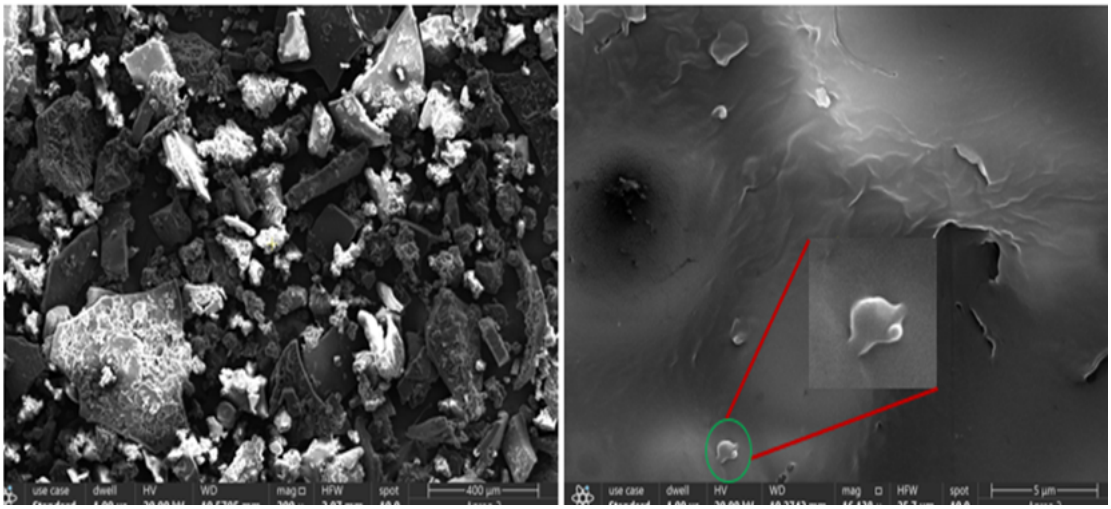

FIGURE 4.10: The surface morphology and topographical features of the micelles.

4.6 ATR-FTIR

To assess any potential interactions between SLM, PLU and ES in the micellar formulation, ATR-FTIR spectroscopy was conducted. The FTIR spectrum of SLM displays several well-defined absorption bands that confirm the presence of important functional groups consistent with its known flavonolignan structure. The O-H stretching vibration of phenolic hydroxyl groups (abundant in the polyhydroxylated flavonoid core) is responsible for strong hydrogen bonding interactions and antioxidant activity, resulting in a broad band at approximately 3410-3390 cm^{-1}.

Moderate peaks at 2925.39 cm^{-1} and 2852.51 cm^{-1} are associated with asymmetric and symmetric aliphatic CH-CH stretching, consistent with saturated methyl (-CH_3) and methylene (-CH_2-) groups found in the flavonolignan side chains; a small peak at 1740.50 cm^{-1} arises from an ester or lactone carbonyl (C=O stretching vibration), which is consistent with the dihydroflavonol core of silibinin and other members of the silymarin complex. Reactive flavonolignan ketone showed a prominent strong peak at 1633.12 cm^{-1} and -OH bending represented by medium intensity absorption at 1362.41 cm^{-1}. Aromatic ring stretching vibrations appeared at two peaks of 1508.87 cm^{-1} and 1454.50 cm^{-1}. The FTIR spectra indicate that the peak at 1085 cm^{-1} is characteristic of flavonolignans, whereas the peak which appears at 994.32 cm^{-1} corresponds to benzopyran ring. From the FTIR spectra, it can be seen that silymarin

mainly contains polyphenolic moiety and confirms its structural vibrational frequencies. The FTIR spectral data corroborate the structure of silymarin which contains hydroxyl-rich aromatic scaffold, ester/lactone carbonyl groups, aliphatic chains, phenolic ethers and is composed of major bioactive flavonolignans: silibinin, silychristin, and silydian.

PLU FTIR spectrum showed, strong sharp peak at 2859.85 cm^{-1} due to asymmetric stretching vibrations of C-H functional groups indicate the presence of alkanes, a signature of the methylene and methyl groups abundant in both PEO and PPO segments, clearly visible is the -CH_2- bending (scissoring) vibration at 1466.19 cm^{-1} indicating linear alkyl chains; peak at 1340 cm^{-1} represents O-H bend. Strong peaks occur for (C-O) carboxylic acids and ethers at 1097.17 cm^{-1} and 1146.02 cm^{-1} respectively, with C-O-C stretching vibrations of ether linkages contributing to the latter absorption peak. The intense band observed at 1097.17 cm^{-1} is assigned to C-O stretching vibrations from the ethylene oxide units in PEO block.

The strong absorption band for ES C=O stretching vibration of ester carbonyl groups at 1725.68 cm^{-1} is characteristic of methyl methacrylate units, and this intense ester carbonyl peak is a spectral signature for polymethacrylates; however, no peak is observed near 1700 cm^{-1} for carboxylic acid carbonyl groups, indicating that most of the acid units exist in their neutral (non-ionized) esterified form consistent with the polymer being in its dry (non-dissociated state).

FTIR spectra reveal O-H stretching vibrations at 2993.98 cm^{-1} and 2951.54 cm^{-1} indicating carboxylic acid. The presence of the multiple methyl substituents on the α-carbon of the methacrylic units is clearly confirmed by C-H bending (deformation) vibrations at 1489.41, 1447.15, and 1387.71 cm^{-1}.

There are several strong absorption bands in the 1260-1150 cm^{-1} region; in particular, there are three strong absorptions at 1263.33, 1191.15, and 1160.02 cm^{-1} that can be attributed to C-O stretching vibrations of ester linkages (typical for alkyl esters) indicating incorporation of methyl methacrylate into the copolymer; the multiple peaks in this region arise from several vibrational modes involving the -C-O-C- groups, as is characteristic of polymethacrylates.

Current formulation (SLM-ES-PLU-Ms) spectrum shows that all the major peaks are retained and no new peak was found. The FTIR spectrum confirmed that all components were present and compatible; it also revealed characteristic peaks, such as a strong ester carbonyl stretching at 1725.86 cm^{-1} due to ES, broad aliphatic -CH_2 stretching around 2881.00 cm^{-1} for Pluronic F127, and the C=C stretching vibration at 1644.12 cm^{-1} and CH_3 bending vibration at 1383.34-1458.34 cm^{-1} as part of the flavonoid structure of Silymarin.

This small peak shows that a minimum quantity of Silymarin remain unentrapped on the surface. The peaks between 1269.94 and 1093.88 cm^{-1} correspond to C-O-C ether linkages for the poly (ethylene oxide) and poly (propylene oxide) blocks of PLU. Bands at 841.13 cm^{-1} and 724.84 cm^{-1} indicate aromatic C-H bending vibrations, consistent with SLM.

Crucially, there are no new peaks or significant shifts present, which would indicate chemical interactions or incompatibilities between the components, nor are any of the peaks significantly broader than expected, confirming that the formulation remains stable and intact.

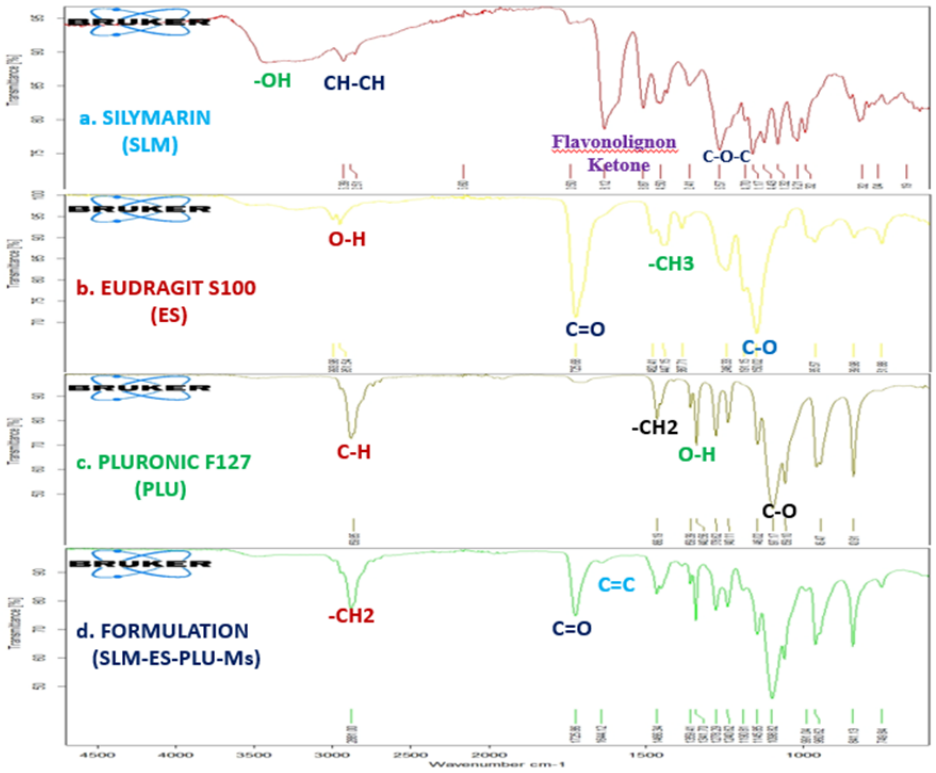

FIGURE 4.11: a. FTIR Silymarin b. FTIR Eudragit S100 c. FTIR Pluronic F127 and Formulation (SLM-ES-PLU-Ms)

4.7 XPRD

XPRD analysis was used to examine the crystallinity and physical state of SLM, PLU, ES and their formulation. As observed in the XPRD patterns, pure SLM shows a broad, diffuse halo, with no sharp peaks, suggesting its amorphous nature, while PLU has multiple intense and sharp peaks between 2θ of 18^o-25^o, which indicates its semi-crystalline nature. However, ES exhibits a broad hump with no sharp peaks that further confirms its amorphous nature. The diffraction pattern for the final formulation shows that the characteristic sharp peaks of PLU are greatly reduced in intensity and broadened, whereas the amorphous halos of SLM and ES were retained, suggesting a partial loss of crystalline structure by PLU most likely as a result of molecular dispersion and physical entrapment of drug and polymer in the matrix. The overall pattern of the formulation indicates reduced crystallinity, which would indicate molecular dispersion of the drug or presence of the drug in an amorphous form, both of which are beneficial to improve solubility and bioavailability. This XPRD profile corroborates development of a physically stable and homogeneous mixture where PLU is rendered non-crystalline and Silymarin remains amorphous, two characteristics necessary for successful drug delivery.

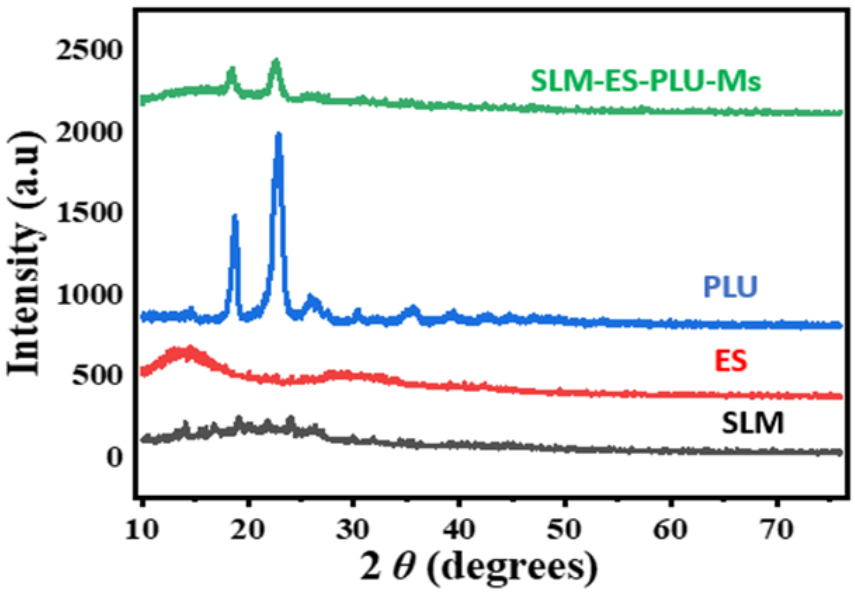

FIGURE 4.12: XPRD of SLM-ES-PLU-Ms, PLU, ES and SLM

4.8 In Vitro Drug Release Study

The simulated fluids including SGF at pH 1.2 and SIF at pH 7.4 were used for the drug release study. SLM-PLU and SLM-ES-PLU-Ms demonstrated the lowest release over the 2-hour period at pH 1.2, accounting for almost 11.45% and 5.04% of the drug release, respectively. Almost both have significant control over the immediate release of the drug over the first two hours in SGF. The drug release pattern of SLM-PLU and SLM-ES-PLU-Ms micelles was maintained at pH 7.4 (SIF).

Approximately 48.04% of the drug was released from SLM-PLU micelles in SIF for 72 hours. In contrast, 99.08% of SLM-ES-PLU-Ms were released in 72 hours.

4.8.1 Statistical Evaluation of Drug Release Profile

The in vitro drug release behavior of SLM-PLU and SLM-ES-PLU-Ms formulations was evaluated under two physiologically relevant pH conditions, which mimic the environment of the gastrointestinal tract: intestinal (pH 7.4) and acidic (pH 1.2). To ascertain the statistical significance of variations in release profiles between the two formulations over time points, comparative analyses were performed. Comparing the release profiles of SLM-PLU and SLM-ES-PLU-Ms at pH 1.2 (an acidic condition) revealed statistically significant variations in the percentage cumulative drug release at each time point (0.5 to 2 hours) ($p < 0.001$). This suggests that, in comparison to the traditional SLM-PLU matrix, the SLM-ES-PLU-Ms formulation significantly altered the early phase release kinetics. In the acidic environment, the increased retention and delayed release point to a protective matrix that might prevent the active compound from degrading or releasing too soon. These results provide evidence that structural modifications, such as the addition of ES and enhancements to the microstructural design of SLM-ES-PLU-Ms, effectively delayed the release of bursts in acidic conditions.

Time points showed statistically significant differences ($p < 0.01$) between the two formulations at pH 7.4. Due to similar polymeric erosion and diffusion mechanisms in

a more favorable environment, this convergence implies that both formulations release the drug in intestinal pH in a comparable manner after initial variations.

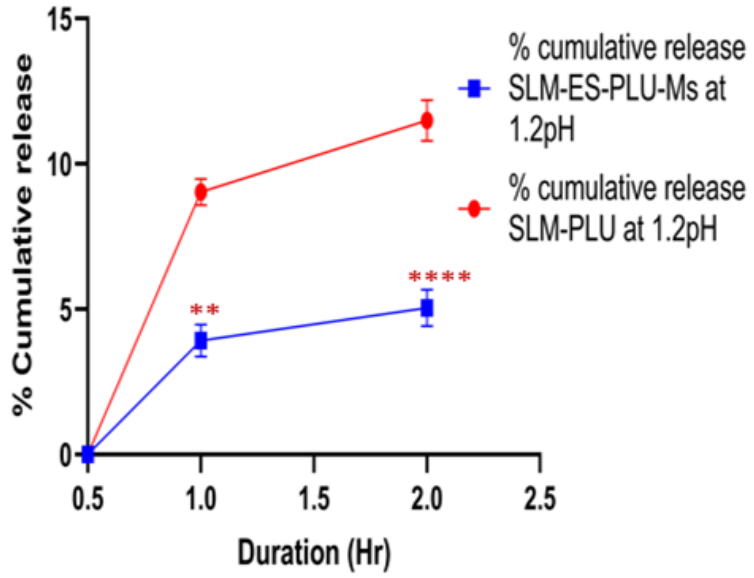

FIGURE 4.13: Graphical Presentation of in vitro drug release at pH 1.2

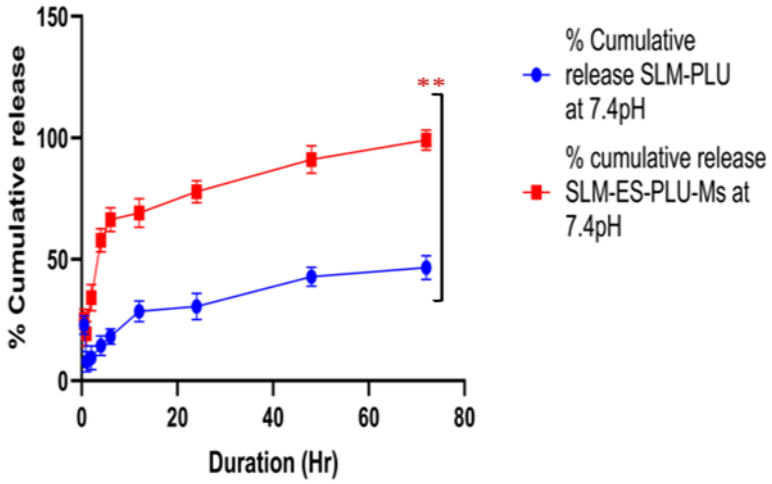

FIGURE 4.14: Graphical presentation of in vitro drug release at pH 7.4

4.8.2 Drug Release Kinetic Modeling

Drug release kinetics modeling was performed, mathematical models describing the drug release kinetics from SLM-PLU and SLM-ES-PLU-Ms at pH 7.4 are shown in table 4.4.

TABLE 4.4: Mathematical models describing drug release kinetics from SLM-PLU and SLM-ES-PLU-Ms at pH 7.4 (SIF). The parameters for the best-fitted models have been shown in the bold.

Silymarin Loaded Pluronic Micelles (SLM-PLU)						
Parameter	**Zero Order**	**First Order**	**Higuchi**	**Korsmeyer-Peppas**	**Hixon-Crowell**	**Peppas-Sahlin**
R	0.9148	0.9495	**0.9807**	**0.9826**	**0.9338**	**0.9910**
R^2	0.5815	0.7590	0.9612	0.9650	0.8715	**0.9820**
RMSE	10.9652	8.3213	3.3404	3.3902	6.4961	2.6240
AIC	63.8201	85.8537	42.4261	43.4893	55.1947	39.4905
MSC	0.3919	0.9438	2.7691	2.6509	1.3503	3.0952
Other	k_o = 0.850	k_1 = 0.013	kH = 6.258	kkp = 7.202, n = 0.461	kHC = 0.003	k_1 = 4.893, k_2 = -0.124, m = 0.697
Silymarin Loaded Eudragit® S100 Coated Pluronic Micelles (SLM-ES-PLU-Ms)						
Parameter	**Zero Order**	**First Order**	**Higuchi**	**Korsmeyer-Peppas**	**Hixon-Crowell**	**Peppas-Sahlin**
R	0.7951	**0.9803**	0.9196	**0.9597**	0.9425	**0.9758**
R^2	-0.1332	0.9490	0.7579	0.9205	0.8832	**0.9517**
RMSE	35.6289	7.5548	16.4680	10.0879	12.2262	8.4959
AIC	85.0318	57.1144	71.1405	63.1172	66.5776	60.6384
MSC	-0.7996	2.3023	0.7439	1.6354	1.2509	1.9108
Other	k_o = 1.839	k_1 = 0.111	kH = 14.329	kkp = 28.804, n = 0.302	kHC = 0.019	k_1 = 22.346, k_2 = -1.281, m = 0.530

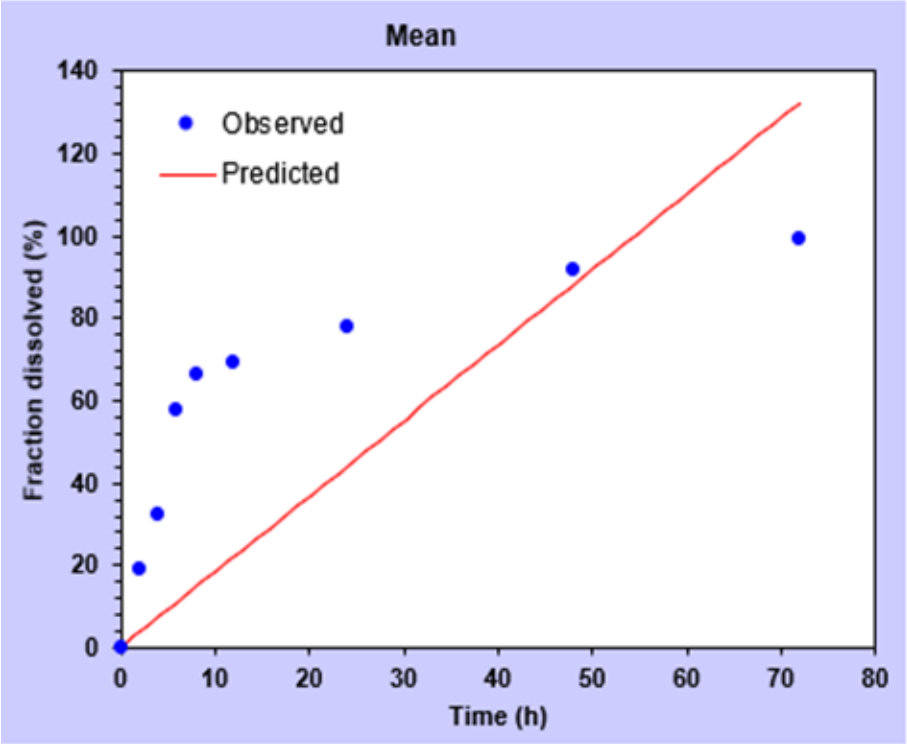

FIGURE 4.15: Graphical presentations of Zero Order drug release kinetics model for SLM-ES-PLU-Ms

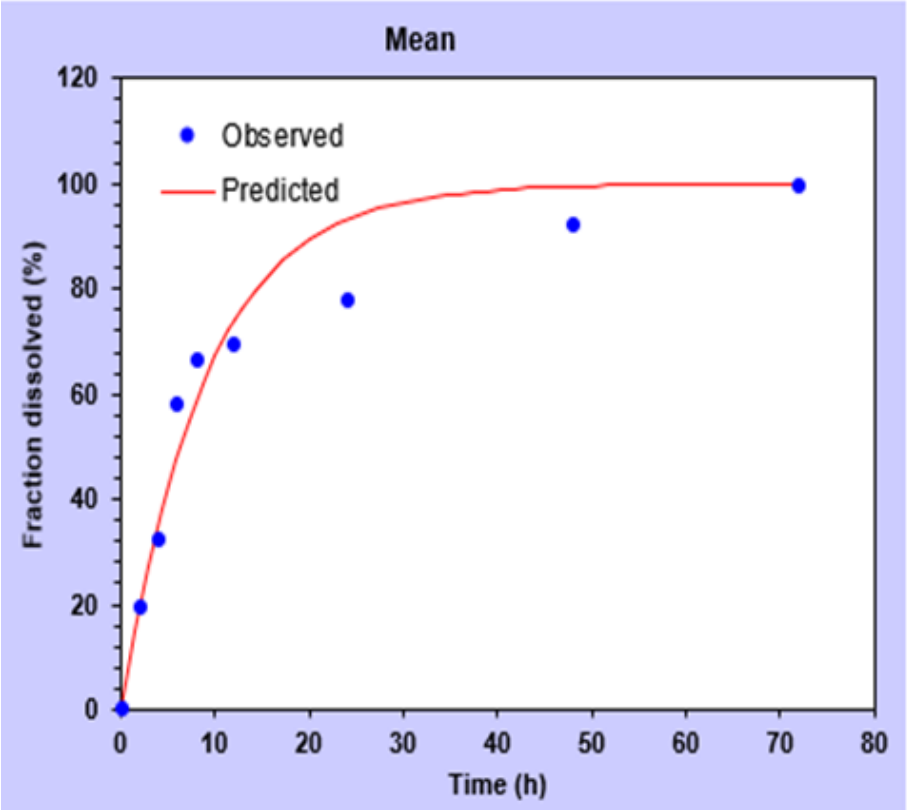

FIGURE 4.16: Graphical presentations of First Order drug release kinetics model for SLM-ES-PLU-Ms

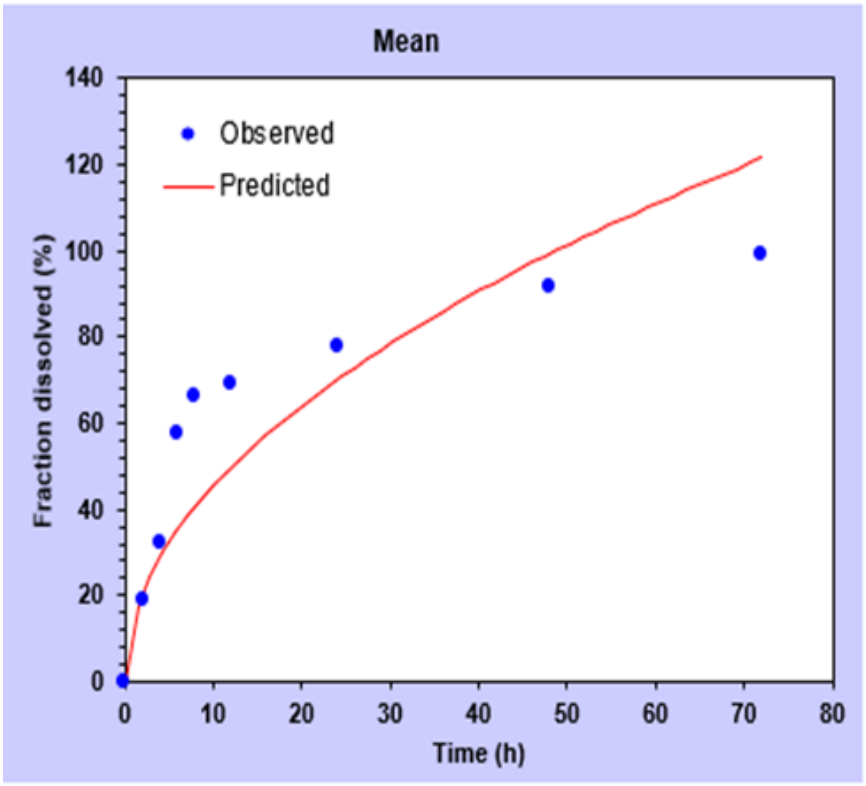

FIGURE 4.17: Graphical presentations of Higuchi model of drug release kinetics for SLM-ES-PLU-Ms

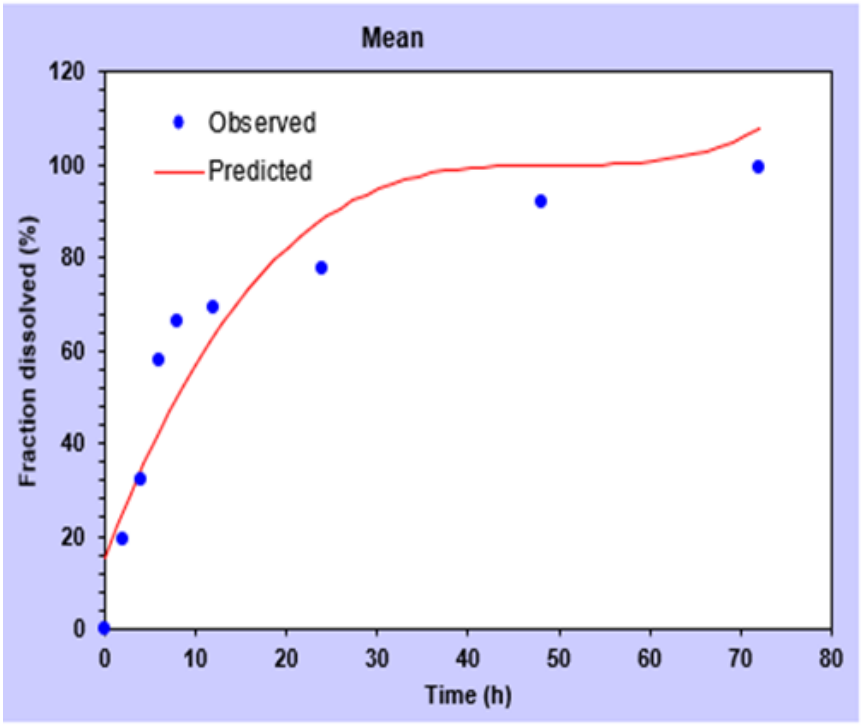

FIGURE 4.18: Graphical presentations of korsmeyer-Peppas model of drug release kinetics for SLM-ES-PLU-Ms

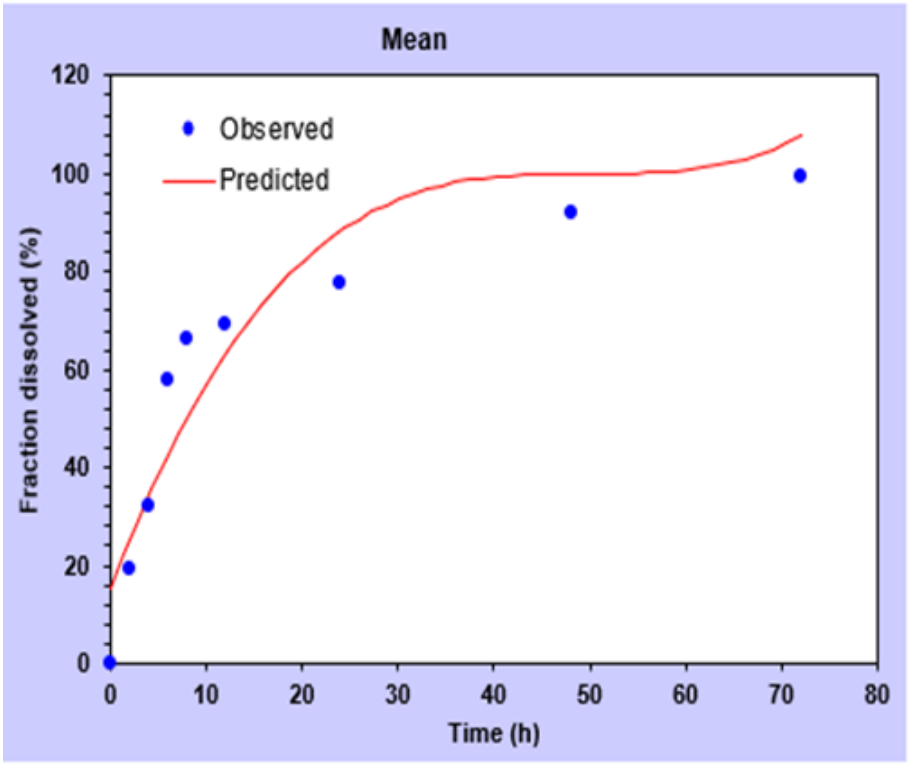

FIGURE 4.19: Graphical presentations of Hixsan-Crowell with Tlag model of drug release kinetics for SLM-ES-PLU-Ms

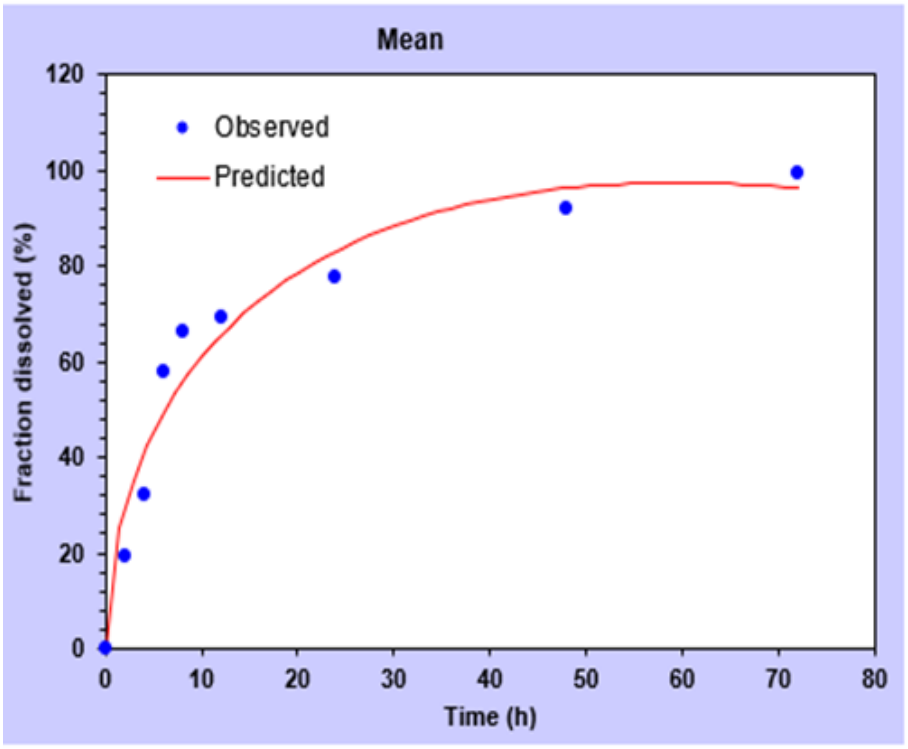

FIGURE 4.20: Graphical presentations of Peppas-Sahlin with Tlag model of drug release kinetics for SLM-ES-PLU-Ms

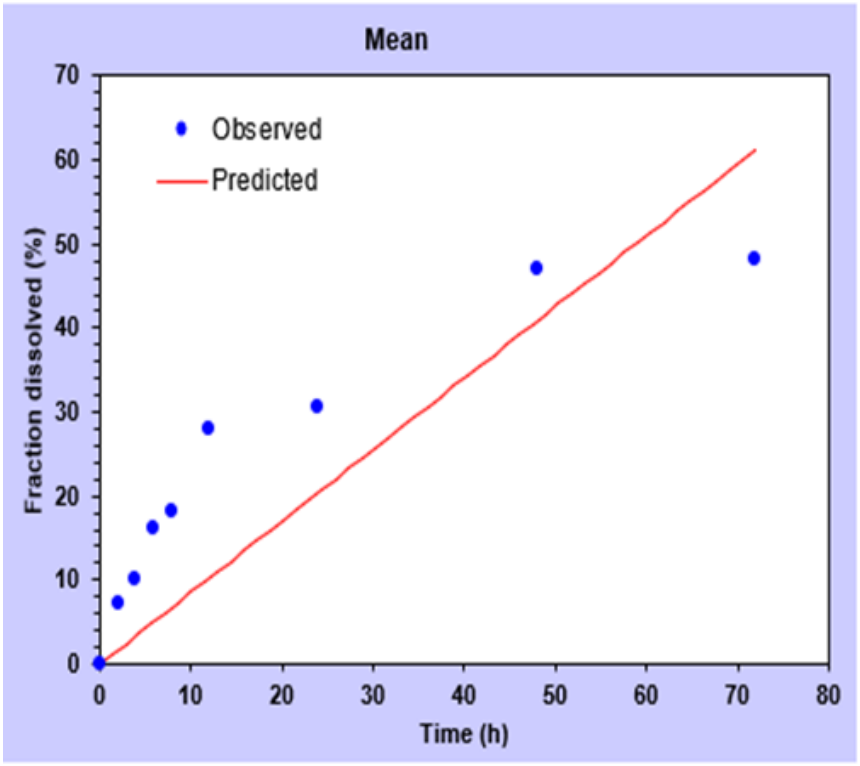

FIGURE 4.21: Graphical presentations of Zero order drug release kinetics model for SLM-PLU

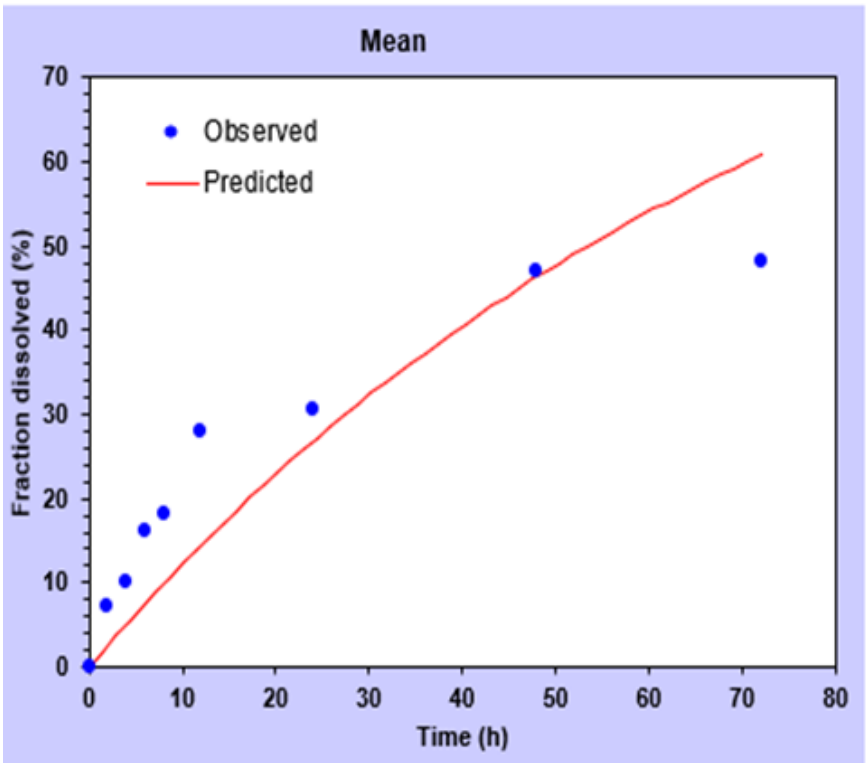

FIGURE 4.22: Graphical presentations of First order drug release kinetics model for SLM-PLU

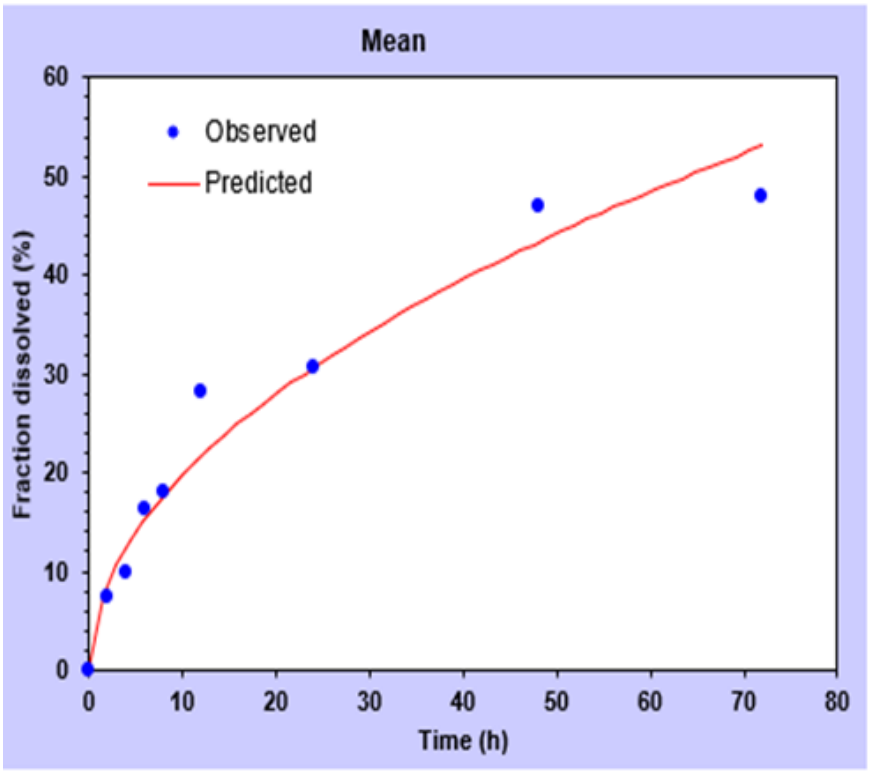

FIGURE 4.23: Graphical presentations of the Higuchi model of drug release kinetics for SLM-PLU

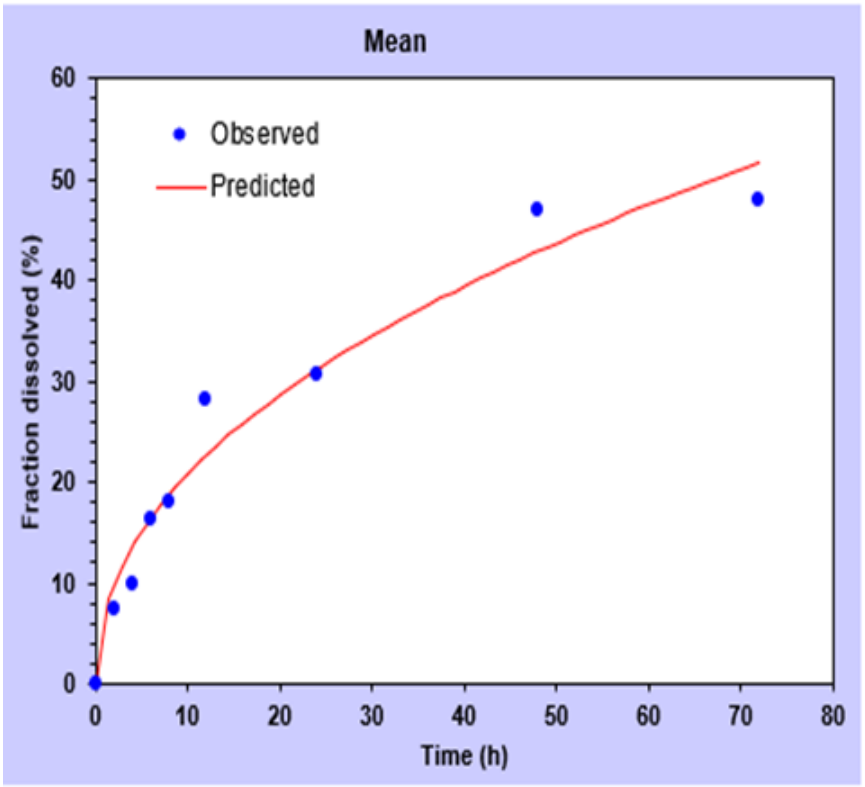

FIGURE 4.24: Graphical presentations of korsmeyer-Peppas model of drug release kinetics for SLM-PLU

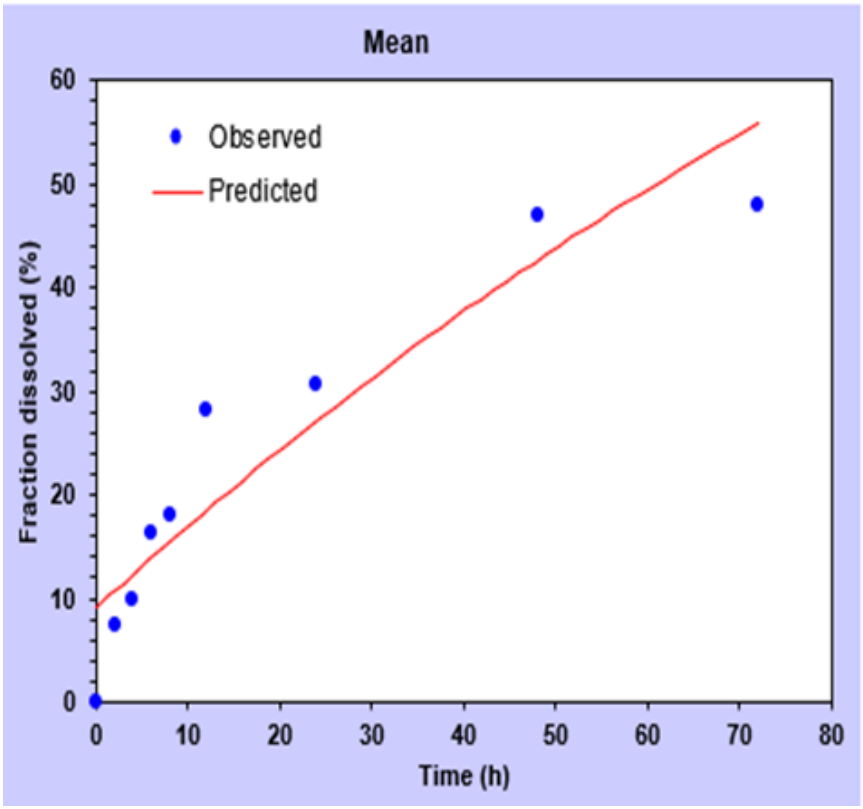

FIGURE 4.25: Graphical presentations of Hixsan-Crowell with Tlag model of drug release kinetics for SLM-PLU

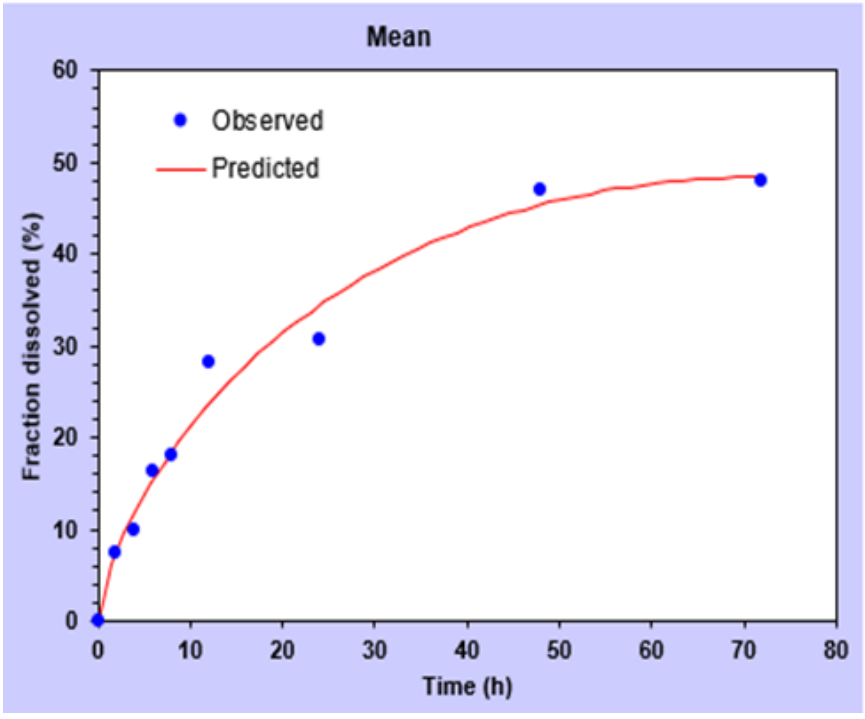

FIGURE 4.26: Graphical presentations of Peppas-Sahlin model of drug release kinetics for SLM-PLU

DD solver was used to perform kinetic modeling of SLM-PLU and Silymarin-loaded SLM-ES-PLU-Ms, evaluating Zero-order, First-order, Higuchi, Korsmeyer-Peppas, Hixson-Crowell, and Peppas-Sahlin release models with model fit assessed using R, R^2, RMSE, AIC, and MSC, which showed the Peppas-Sahlin model to perform best for both SLM-PLU and SLM-ES-PLU-Ms formulations. The Peppas-Sahlin model was found to be consistently better than other models, followed by First-order kinetics and then Second-order kinetics; the Peppas-Sahlin model gave an R of 0.9910, R^2 of 0.9820, RMSE of 2.624, AIC of 39.49, and MSC of 3.0952 for SLM-PLU; while First-order kinetics provided a good fit (R = 0.9803) with R^2 of 0.952 for SLM-ES-PLU-Ms.

This suggests that the Peppas-Sahlin model best describes the drug release mechanism for both formulations. The coefficients of this model also give mechanistic insight; in both cases $k_1 > k_2$ (SLM-PLU: k_1 = 4.893, k_2 = -0.124; SLM-ES-PLU-Ms: k_1 = 22.346, k_2 = -1.281), and the mechanism of diffusion is more significant than that of polymer relaxation, which is in line with the exponent values (m = 0.697 and n = 0.461) that indicate anomalous but predominantly Fickian diffusion mechanism, although m is slightly higher than n in this formulation, both are well below the theoretical cutoff for Case-II transport (i.e., 0.89), which indicates minimal contribution from polymer relaxation; it also supports the observation that both models describe. This is consistent with the values observed for the Korsmeyer-Peppas model release exponent (n = 0.461 for SLM-PLU and n = 0.302 for SLM-ES-PLU-Ms), which are both below 0.5, as predicted by drug release kinetics theory.

Notably, the ES coated formulation SLM-ES-PLU-Ms showed significantly higher k_1 values than all other formulations, which could be attributed to a more pronounced diffusion-driven release profile, with possibly additional pH-sensitive dissolution of the Eudragit® coating at intestinal pH. Even for this coated system, it is still largely diffusion-based, albeit more complicated as indicated by the relatively low n-value and negative k_2 value.

This study indicates that silymarin release from both micellar systems follows Fickian diffusion, and Peppas-Sahlin and Korsmeyer-Peppas models are suitable mathematical descriptions of the release kinetics.

4.9 Stability Studies

Stability studies were conducted according to ICH guidelines for accelerated (25 ^{o}C ± 2 ^{o}C and 60 ± 5 % relative humidity; RH) versus refrigerated (5 ^{o}C ± 3 ^{o}C) conditions for 30 days. Stability studies are crucial for determining the impact of storage conditions on the performance of nanocarrier systems; key parameters that determine colloidal stability and affect shelf life, efficacy, and safety profile are particle size, PDI, and zeta potential.

4.9.1 Stability at (5 ^{o}C ± 3 ^{o}C)

The formulation had an initial mean particle size of 42.80 nm, a PDI of 0.182, and a zeta potential of -42 mV; after 30 days at 2-8 ^{o}C, the particle size slightly increased to 45.48 nm, while the PDI decreased slightly to 0.178, but most notably, the zeta potential changed significantly to -42 mV. The average particle size increase (6.3%) was low, indicating no significant aggregation or coalescence, PDI was less than 0.2 (optimal value for nano-formulations), and there was a sharp rise in the magnitude of zeta potential from -42 mV to -8.42 mV due to structural reorganization at the particle surface or delayed ionization of surface groups during cold storage, which further enhanced inter-particle repulsion and improved dispersion stability, suggesting refrigerated storage is favorable for maintaining the colloidal integrity of the nanoparticles. These results imply that refrigerated storage preserves the colloidal stability of the nanoparticles.

4.9.2 Stability at (25 ^{o}C ± 2 ^{o}C and 60 ± 5 % Relative Humidity; RH)

At room temperature (25 ^{o}C) promotes a significant loss of colloidal integrity after 30 days, with an increase in particle size from 42.80 nm to 75.92 nm (a 77.4% increase), minor rise in PDI from 0.182 to 0.193, and improvement of the zeta potential to -35 mV, which suggests incipient aggregation due to increased Brownian motion or weak

surface stabilization at room temperature Even with increased particle size, the PDI remained low (below 0.2), indicating that the system did not become highly polydisperse but likely aggregated into larger aggregates of uniform size. The zeta potential of -35 mV is much more positive than the initial -8.42 mV but still within the electrostatically stable range (—±30 mV— and above), suggesting that some surface level stabilization occurred, but it was not enough to keep particles from aggregating at higher temperatures. These results suggest that storage at room temperature compromised nanoparticle size and uniformity despite the fact that electrostatic repulsion had improved; kinetic energy at 25 ^{o}C probably overcame repulsive forces to enable particle collision and fusion.

TABLE 4.5: Stability Studies

Parameter	**Initial Results**	**After 30 Days (5 ^{o}C ± 3 ^{o}C)**	**After 30 Days (25 ^{o}C ± 2 ^{o}C, RH: 60% ± 5%)**
Particle Size (nm)	42.80	45.48	75.92
Zeta Potential	-42	-8.42	-0.35
PDI	0.182	0.178	0.193

Refrigerated storage (2-8 ^{o}C) clearly preserved both particle integrity and distribution while increasing zeta potential significantly; room temperature (25 ^{o}C) resulted in significant particle growth, although with a still favorable zeta potential for electrostatic stability. The data suggest that 2-8 ^{o}C is the preferred storage condition for this nano-formulation, which results in increased electrostatic repulsion and minimal physicochemical changes over 30 days, whereas room temperature leads to significant particle size increase which could affect product performance and shelf-life; hence cold-chain conditions are essential for long-term stability of such a nano-formulation and clinical applicability.

4.10 In Vivo Studies

The anti-inflammatory effects of SLM-ES-PLU-Ms were evaluated on the DSS induced colitis animal model. Symptomatic parameters like loss in bodyweight, stool consistency and rectal bleeding were monitored on daily basis and graded from zero to four to attain DAI score according to below tables [50].

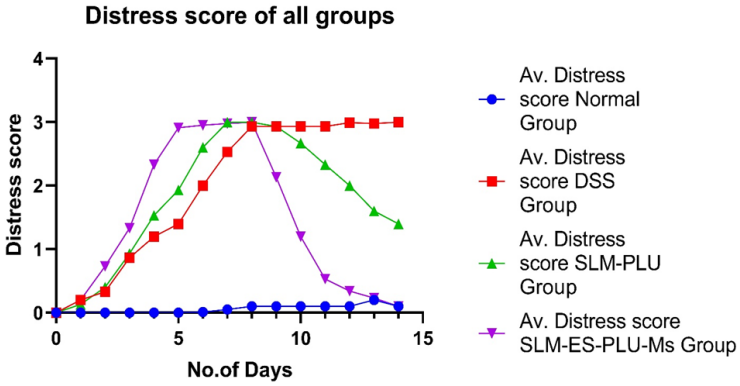

FIGURE 4.27: Distress score of Normal Group, DSS Group, SLM Group and SLM-ES-PLU-Ms Group

The resulting distress scoring graph indicated that while there were no statistically significant differences between groups in their baseline levels of anxiety (or stress), the experimental groups had significantly higher scores on the anxiety and stress scales following treatment with DSS, indicating that not only did the DSS induced condition result in a physiological response but it also resulted in increased behavioral and emotional states (the SLM-ES-PLU-Ms treatment group had markedly lower levels of anxiety and stress than the DSS group). The SLM group experienced significantly less distress than the DSS group but more than the SLM-ES-PLU-Ms treatment group, indicating that this formulation had some degree of behavioral protection. In addition, the normal (control) group have consistently lower distress scores, which served as a baseline for healthy behaviors.

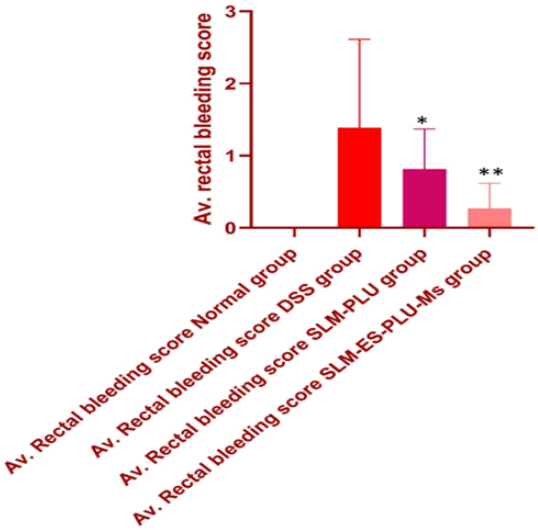

FIGURE 4.28: Av. Rectal bleeding score of Normal Group, DSS Group, SLM and SLM-ES-PLU-Ms Group

Rectal bleeding score is more in DSS group, relatively less in SLM-PLU group and significantly less in SLM-ES-PLU-Ms group.

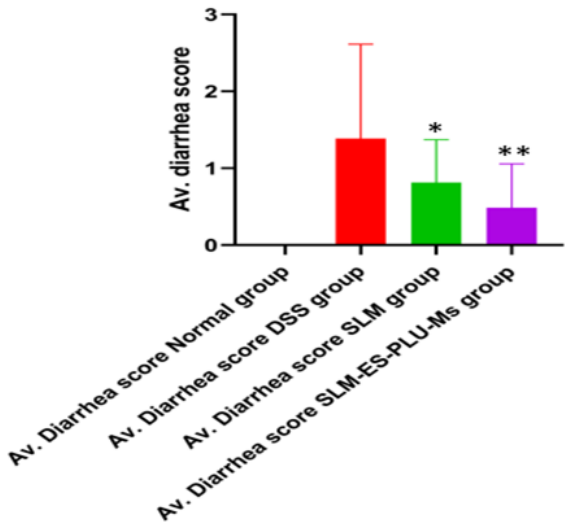

FIGURE 4.29: Av. diarrhea score of Normal Group, DSS Group, SLM and SLM-ES-PLU-Ms Group

Diarrhea score is more in DSS group, relatively less in SLM group and remarkably less in SLM-ES-PLU-Ms group.

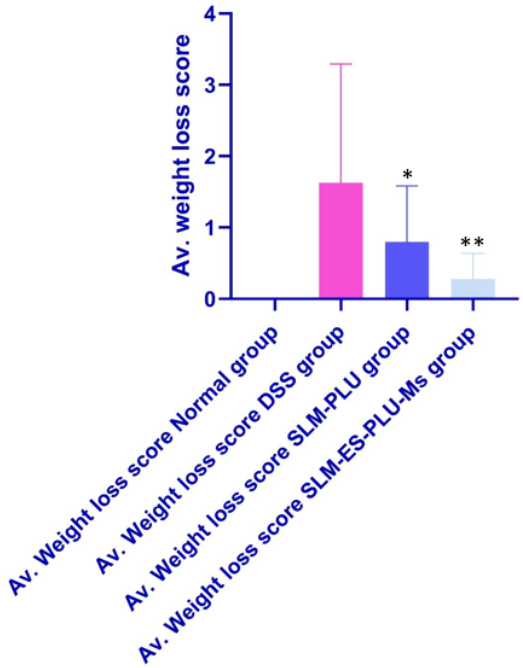

FIGURE 4.30: Av. Weight loss score of Normal Group, DSS Group, SLM and SLM-ES-PLU-Ms Group

Weight score is more in DSS group, relatively less in SLM-PLU group and remarkably less in SLM-ES-PLU-Ms group.

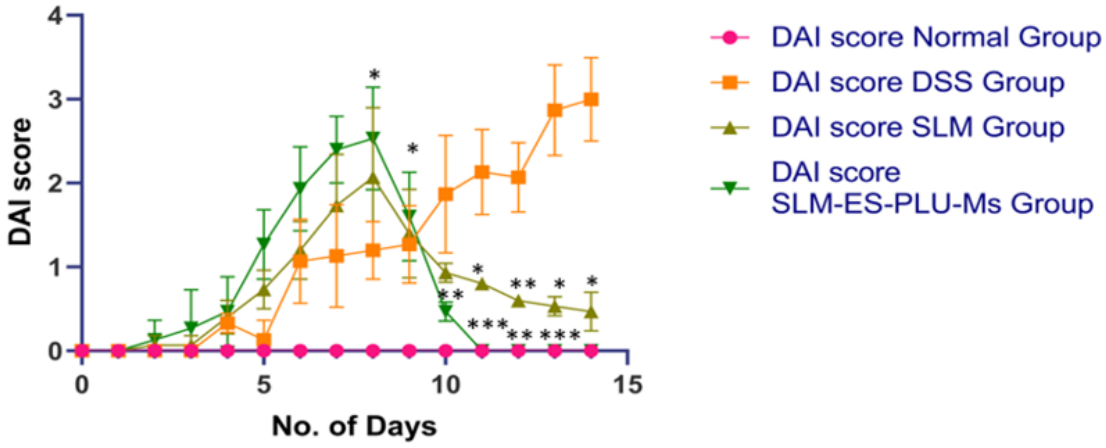

FIGURE 4.31: DAI score of Normal Group, DSS Group, SLM and SLM-ES-PLU-Ms Group

DAI score of normal group is zero as indicated in Figure 4.31, highest DAI score observed in DSS group, free drug group (SLM) showed improved DAI score after eighth day, however there was significant improvement in DAI score of formulation (SLM-ES-PLU-Ms) treated group indication of efficacy of SLM-ES-PLU-Ms.

4.10.1 Macroscopic Assessment of Disease Severity and Formulation Efficacy

Colon shortening is a well-known macroscopic indicator of inflammation in experimental models of IBD, as obvious in mice with DSS induced colitis. This visual metric is a clear indicator of the course of the disease and the effectiveness of treatment because it correlates with edema, immune cell infiltration, and mucosal damage.

The colon is uniformly shaped, appears long (10.88 cm), and shows no signs of thickening or lesions. This is in line with the architecture of healthy, non-inflammatory tissue. The baseline is this group. There is a noticeable shortening of the colon (about 7.36 cm) and several dark, enlarged, and thickened sections. These alterations are a sign of severe colonic edema and inflammation, which are frequently linked to colitis brought on by DSS. Immune cell infiltration and mucosal ulceration are further

supported by the presence of numerous nodular lesions. There is a noticeable partial recovery of colon length (8.74 cm). There are still some dark areas, but not as many as in the DSS group. This shows that by lessening the degree of inflammation and maintaining tissue integrity, SLM treatment likely a therapeutic intervention or scaffold offers moderate protection or therapeutic benefit. Among the treated groups, this group shows the biggest improvement, with colon length approaching normal levels (10.04 cm). Lesions are visible in smaller and fewer numbers, suggesting that colonic inflammation has been effectively suppressed. The synergistic anti-inflammatory effect is probably improved by the SLM-ES-PLU-Ms complex (possibly a combination therapy or altered delivery system).

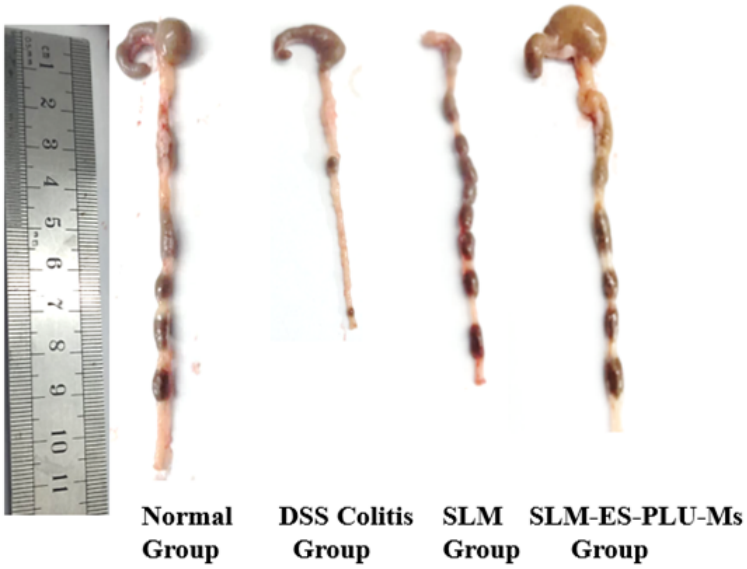

FIGURE 4.32: Colon length comparison in different groups

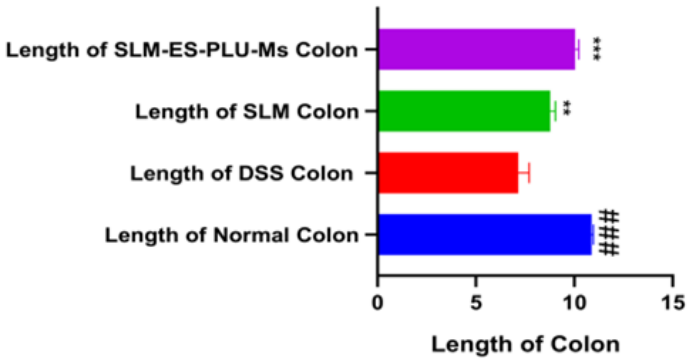

FIGURE 4.33: Assessment of colon lengths of mice of different groups (n=3) collected at the end of experiment (Day 14)

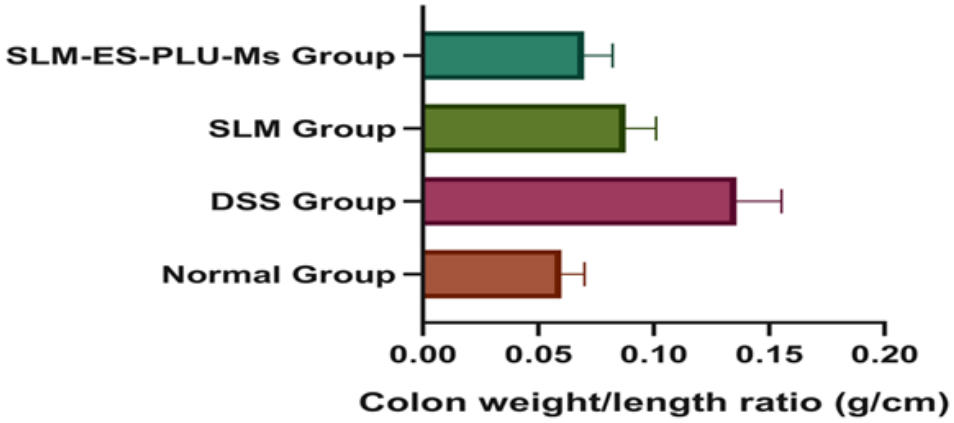

FIGURE 4.34: Assessment of colon weight/length ratio of mice of different groups (n=3) collected at the end of experiment (Day 14)

4.11 Histological Analysis

Histological examination of all four groups can be observed from Figure 4.35 to 4.38. The normal colon was not inflamed (Figure 4.35). No disruption of crypts observed.

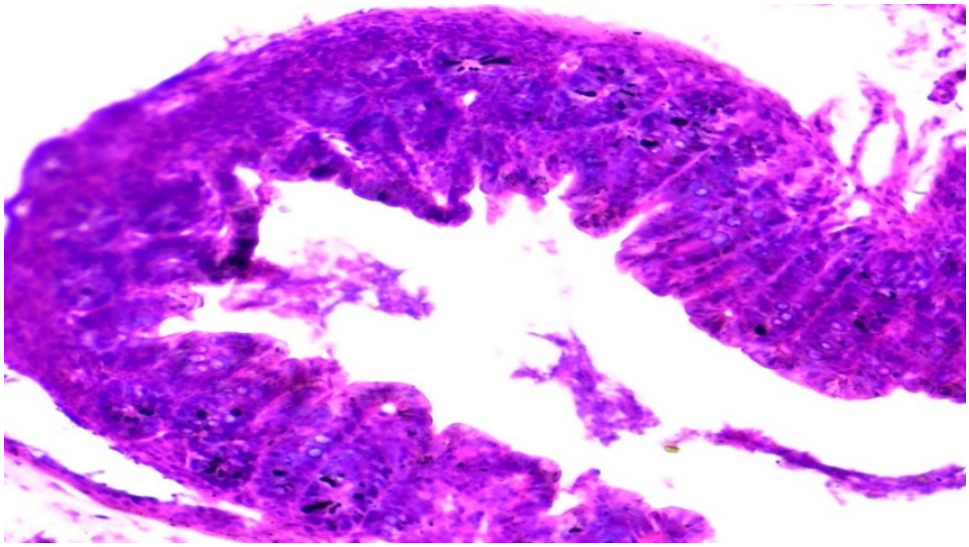

FIGURE 4.35: Normal Colon

In a DSS group (Figure 4.36), a significant number of dark-staining small nuclei are dispersed throughout the mucosa and lamina propria. These likely represent lymphocytes, macrophages, and potentially plasma cells, consistent with chronic inflammatory infiltration. Disrupted, irregular arrangement of crypt structure indicating chronic inflammation.

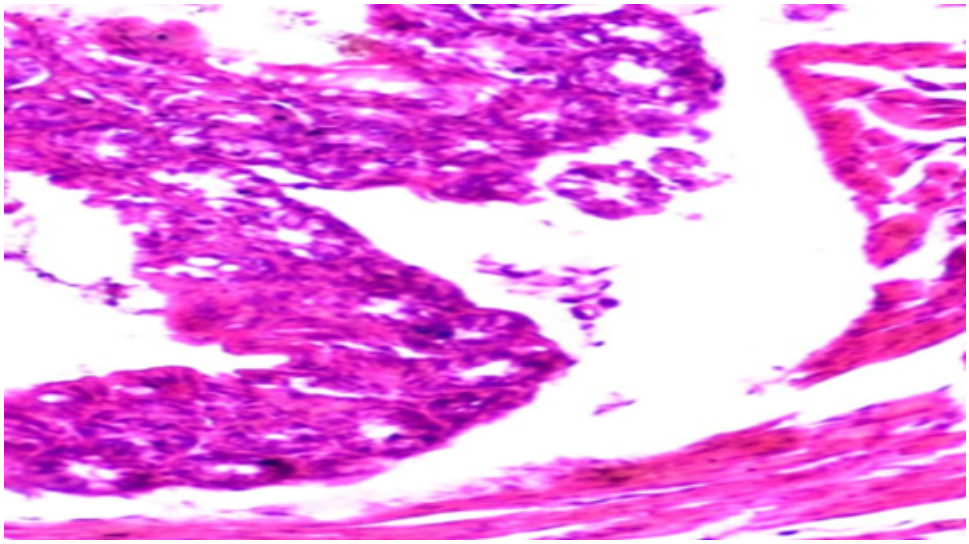

FIGURE 4.36: DSS Group Colon. Arrow indicates immune cells

In SLM drug treated group, crypts appear intact, there is some architectural distortion and immune cells that could suggest ongoing repair or regenerative activity which would be consistent with treated or resolving inflammation.

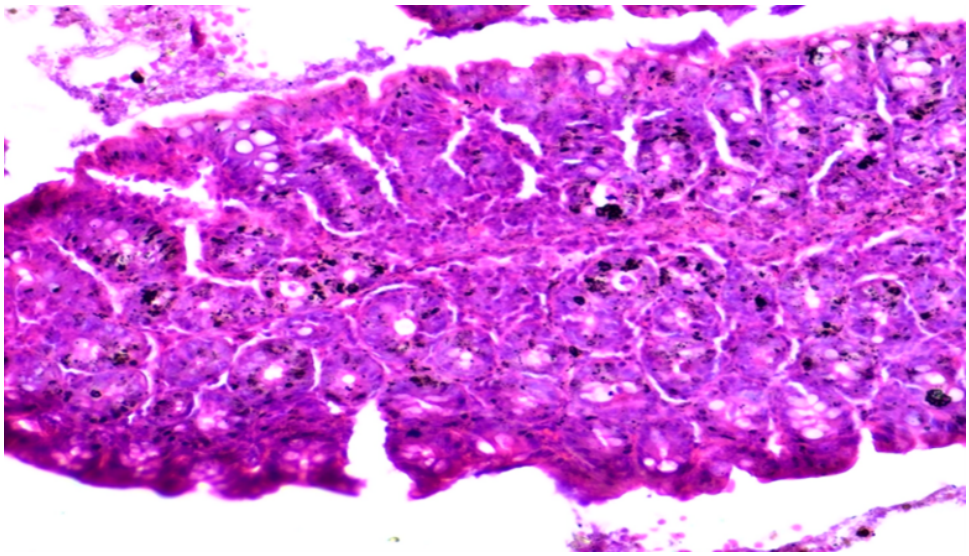

FIGURE 4.37: SLM Group

In SLM-ES-PLU-Ms treated group (Figure 4.38), submucosa shows organized non-edematous connective tissue with elongated fibroblasts and collagen bundles; no signs of neutrophil infiltration, hemorrhage or fibrosis indicative of chronic or acute inflammation; no inflammatory infiltrate in the lamina propria or submucosa. A few dark granules are visible but sparse and may represent treatment-related particles.

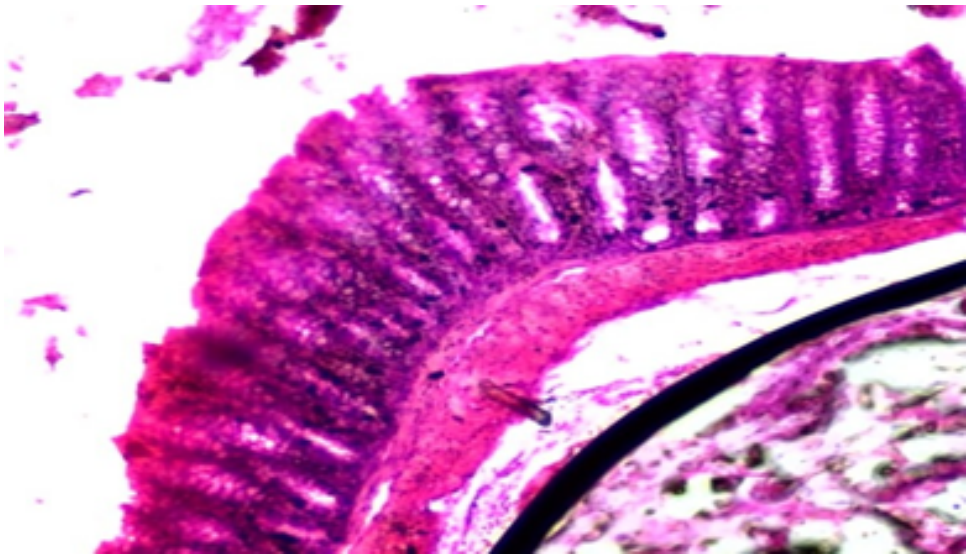

FIGURE 4.38: SLM-ES-PLU-Ms Group

The mucosa and lamina propria contain a sizable number of tiny, dark-staining nuclei. In line with chronic inflammatory infiltration, these most likely represent macrophages, lymphocytes, and possibly plasma cells.

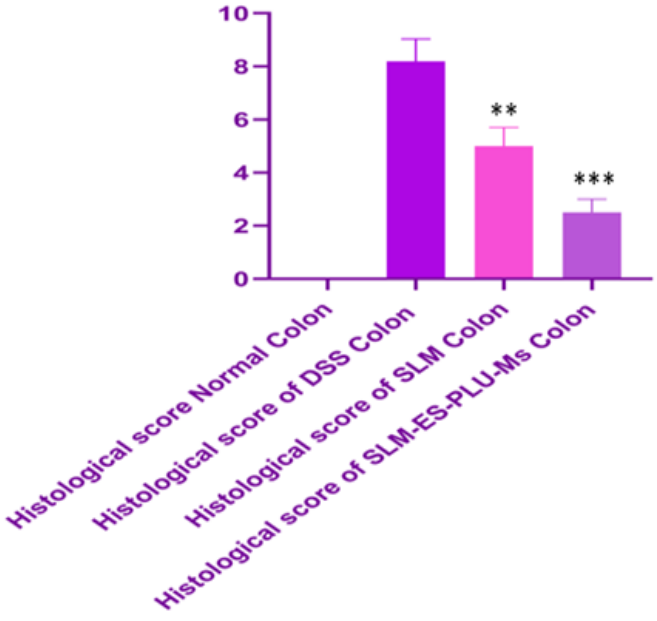

FIGURE 4.39: Histological score of Normal colon, DSS colon, SLM treated colon and SLM-ES-PLU-Ms treated colon

The histological score in the normal group was close to zero, indicating that there were no pathological changes and that the colon's physiological morphology was at

its baseline. On the other hand, the DSS group had a significantly higher histological score 8 ± 0.5, which was indicative of severe mucosal ulceration, widespread epithelial necrosis, and crypt distortion. Following SLM treatment, the histological score decreased by 5 ± 0.6, indicating a partial restoration of epithelial integrity and a reduction in inflammatory changes. Notably, the group treated with SLM-ES-PLU-Ms showed the greatest histological improvement, with a histological score that decreased to about 2.8 ± 0.4. This suggests that the SLM-ES-PLU-Ms successfully reduced the mucosal damage induced by DSS and encouraged the structural restoration of colonic tissues.

Chapter 5

Conclusion

The current study successfully developed and characterized a pH-responsive Pluronic micelle-based drug delivery system for targeted treatment of inflammatory diseases in the intestines, emphasizing the enhancement of the therapeutic possibility of SLM. The formulation showed substantial improvements in drug solubility, stability, and delivery and to tackle the biopharmaceutical barriers of SLM's poor aqueous solubility, oral bioavailability and instability in the gastric environment. We have designed and optimized a pH-responsive PLU micelles-based drug delivery system coated with ES to improve the oral delivery of silymarin to the pathological site of inflammation for IBD, specifically UC. The developed formulation resolved important factors that contributed to SLM's poor water solubility, low permeability (BCS Class IV), rapid first-pass metabolism, and instability in the gastric environment. SLM-PLU-Ms were developed using a direct dissolution method and were further coated with ES (SLM-ES-PLU-Ms) to produce pH-responsive drug release characteristics. The amphiphilic characteristics of PLU micelles allowed SLM to show significant increases in aqueous solubility and permeability, as SLM has poor absorption due to being BCS Class IV. By placing SLM into a hydrophobic micellar core and covering it with a hydrophilic shell, the formulation was able to avoid any limitations associated with poor dissolution and enzymatic degradation in the upper GIT, greatly improving bioavailability by providing a sustained and controlled release at the disease site.

In Vivo pharmacodynamic study in the DSS-induced mice colitis model clearly demonstrated the efficacy of the optimized micellar system. SLM-ES-PLU-Ms treated mice group showed clear improvements in histopathology parameters, including declining colon shortening, normalizing colon architecture, reduced DAI scores, preserving mucosal integrity. Optimization using Design Expert® software demonstrated that the three factors' studies (polymer concentration, homogenization speed and stirring time) affected the properties of the micelles. The ideal formulation (Run 6) had an average particle size of 42.80 nm, polydispersity index (PDI) of 0.182, and zeta potential of -42 mV, indicative of excellent colloidal stability.

The size, PDI and zeta potential are all critical parameters to ensure efficient drug loading, increased circulating times and target delivery to the inflamed tissues of the intestinal tract. Particle Size and PDI nanoscopic size ($\sim$100 nm) and low PDI values (< 0.5) would maximize passive targeting and accumulation at the inflamed sites in the colon with the EPR phenomena. Zeta potential negative surface charge of the SLM-ES-PLU-Ms (-42 mV) provided electrostatic stabilization to the micelles, which would all lower the chance or occurrence of aggregation, and early interactions resulting in statically guided drug release during systemic circulation.

The EE of the SLM-ES-PLU-Ms was 79.63%, higher in comparison to uncoated micelles (72.26%). The improvement was likely due to the ES, which provides an additional barrier to drug leakage and strengthens the micelles. The large EE highlights the formulation's ability to solubilize and protect the BCS Class IV drug SLM from degradation in the harsh GI environment.

Morphological Analysis (SEM) images display semi-spherical and spherical micellar structures that are smooth in regard to morphology. Their presence confirms the success of self-assembly. Crystalline domains not observed meaning the system can be interpreted as the drug being amorphous which is better for solubility and dissolution. ATR-FTIR spectra showed no possibility for chemical interactions to occur between SLM, PLU and ES, as all required characteristics were retained, demonstrating compatibility. Important functional groups including the phenolic hydroxyl group and the ester carbonyl group were retained, ensuring drug stability. X-ray Powder Diffraction (XPRD) amorphous nature of the silymarin drug in the formulation was confirmed

due to the absence of sharp crystalline peaks, providing further evidence for better drug solubility and improved bioavailability.

The drug release profile was determined in simulated acidic (pH 1.2) and neutral (pH 7.4) environments altogether with good results, pH 1.2 (SGF): A total of only 5.04% of SLM was released from SLM-ES-PLU-Ms over the two-hour period, showing that acidic degradation was adequately protected against and good to allow for any drug release in the acidic environment of the stomach to be addressed. PH 7.4 (SIF), 99.08% sustained release over 72 hours with appropriate pH response indicative of the successful demonstration of pH-triggered release of drug in polylecitine colorectal delivery. The Peppas-Sahlin drug release kinetics model fitted our data very well ($R^2 = 0.952$) indicating predominantly a diffusion-based mechanism with minimal polymer relaxation. Additionally, the Korsmeyer-Peppas exponent (n = 0.302–0.461) was consistent with anomalous (non-Fickian) diffusion in that while diffusion does happen so too does polymer erosion with respect to swelling, layer dissolution, and erosion.

The anti-inflammatory efficacy of SLM-ES-PLU-Ms was assessed in a murine model of UC induced by DSS, DAI significantly lower DAI scores (weight loss, stool consistency, rectal bleeding) were found when comparing SLM-ES-PLU-Ms treated mice with both DSS control and free SLM treatment groups. Macroscopic Parameters Colon length retention and lower spleen mass in the group receiving SLM-ES-PLU-Ms suggested a decrease in the inflammation and tissue damage seen in UC. Behavioral metrics, SLM-ES-PLU-Ms lowered distress scores, and suggested the formulation can decrease the distress associated with colitis. These data indicate the superior therapeutic effect of the micellar system compared to free silymarin likely due to improved bioavailability, a targeted delivery route and extended action of the drug released in the inflamed area.

The formulation exhibited remarkable physicochemical stability over a duration of 30 days at refrigerated ($5^oC \pm 3^oC$) environments, with no notable changes to particle size, polydispersity index (PDI), zeta potential, or drug content. Altogether, the stability results have demonstrated the appropriateness of the formulation for extended storage and clinical scale-up. The stability for ICH-recommended conditions confirms

the micellar system's structural fidelity and resilience to aggregation, leaking, and degradation over time. Both accelerated (25^{o}C, 60 % RH). Refrigerated (5^{o}C $\pm$ 3^{o}C) conditions demonstrated excellent physicochemical stability of the formulation over 30 days with no significant changes in particle size, polydispersity index (PDI), zeta potential. The stability data presented in this study support the long-term stability of the formulation and its potential for scale up for clinical studies. The stability demonstrated in an ICH recommended stability study confirms micelles stability, and the ability of the formulation to remain stable in terms of structural integrity, without aggregation, leakage or degradation over time. In pH-responsive targeted delivery system, the addition of ES conferred site specific release characteristics to the formulation. Drug release was observed to be minimal under gastric (pH 1.2) conditions, while enhanced drug release was observed under colonic conditions (pH $>$ 7.0). while enhanced drug release was observed under colonic conditions (pH $>$ 7.0). This pattern of targeted delivery gave the formulation the capacity to minimize premature drug degradation and systemic absorption and reduce toxicity risk, while providing a safer and more efficacious therapeutic profile aligned with the indications for drugs delivered with colon-specific drug delivery systems. Improved bioavailability and permeability PLU micelle's amphiphilic properties enabled significant increases in SLM aqueous solubility and permeability. SLM is classified as BCS Class IV and is poorly absorbed. SLM was encapsulated in a micellar hydrophobic core and protected in a hydrophilic shell, and eventually broke down resistance to poor dissolution and enzymatic degradation in the gut.

5.1 Future Prospective

Level of proinflammatory cytokines TNF α, IL-1β and IL-6 would be quantified for all the groups including normal group, DSS group, free drug treated group and formulation treated group. For further enhance the specificity of the micelles, future research could utilize dual targeting strategies utilizing passive targeting (EPR effect) and active targeting. Micelles could be conjugated with ligands such as folic acid (for overexpression of folate receptor-α in IBD) or antibodies against MAdCAM-1

to target gut-associated lymphocyte homing, which would increase the accumulation of micelles in inflamed tissues. Additionally, mucoadhesive polymers chitosan or thiolated Eudragit could provide longer residence times in the colon due to interactions with mucus layers. One further unique idea would be to use bioresponsive linkers, which are sensitive towards reactive oxygen species (ROS) or matrix metalloproteinases (MMPs- frequently found in IBD lesions), allowing for spatially restricted drug release.

Through the multifactorial nature of IBD, combined therapies could enhance therapeutic efficacy. Co-encapsulation of SLM with curcumin (another anti-inflammatory polyphenol) or 5-aminosalicylic acid (5-ASA) may have additive or synergistic effects. Another method is using probiotic-loaded micelles that can deliver anti-inflammatory medications and beneficial bacteria (*Faecalibacterium prausnitzii*) together to restore homeostasis in the gut microbiota. For a more difficult to treat patient, we may consider small-molecule inhibitors (e.g., JAK/STAT inhibitors) that target resistant pathways for inflammation.

Advances in stratifying patients could yield personalized micellar formulations for patients based on a disease subtype (e.g., Crohn's vs UC) or biomarker profile (e.g., high TNF-α vs. IL-23 predominance). Additionally, 3D printed dosage forms containing micelles could allow for custom doses, while point-of-care diagnostics (fecal calprotectin tests) could facilitate treatment adaptation. Alternatively, machine learning-based algorithms could evaluate patient detail to recommend optimal drug ratios or release profiles. To enhance oral bioavailability needs to address both mucus penetration and intestinal permeability. PEGylation or mucolytic agents (e.g., N-acetylcysteine) could provide improved diffusion through mucus as well as permeation enhancers (e.g., sodium caprate) could aid in epithelial uptake; of systemic use, stealth coatings (e.g., PEG or mimetics of CD47) could also evade immune clearance, thus increasing the length of circulation half-life. Regulatory and Manufacturing Issues, problem with scaling up involves batch-to-batch variability in micelle size and drug loading when increasing from small-scale synthesis. While microfluidic synthesis would allow more exact control over the production as well as potential for larger scale, this must be balanced with cost. Regulatory authorities will expect comprehensive

documentation from the start, including stability data generated using locality of the applicable ICH guidelines. Additionally, bioavailability should be conducted versus established SLM product (e.g. Legalon®) before approvals can occur.

The current pH-responsive micellar delivery platform for intestinal inflammation highlights the flexibility and versatility of polymeric micelles for various inflammatory and chronic disease states beyond IBD. While developing these nanocarriers can lead to many organ-specific diseases that have open unmet needs in targeted delivery, increased solubility and controlled release. Liver Disease target Hepatic stellate cells (HSCs) in Fibrosis Chronic liver disease are a global health burden, specifically hepatic fibrosis.

HSCs are essential in liver fibrogenesis following activation, overproducing extra cellular matrix (ECM). Engineering ligand-functionalized polymeric micelles that bind to receptors highly expressed on activated HSCs (e.g., Platelet-derived growth factor receptor beta (PDGFR-β) or integrins) would potentially enhance the targeted delivery of antifibrotic agents, nucleic acids siRNA against TGF-β signaling) or antioxidants with the aim of reversing the natural progression of fibrosis while sparing healthy hepatic cells. This approach represents an area of recent research focusing on hepatic-targeted nanomedicine to improve drug activity while reducing off-target effects for chronic liver disease. 6.2 Skin Diseases: Topical Micellar Systems for Psoriasis and Atopic Dermatitis The utility of polymeric micelles presents a good opportunity for a topical drug delivery system in chronic skin diseases such as psoriasis or atopic dermatitis.

As the developments in nanomedicine continue to cascade and gain recognition, it is crucial to develop with an environmental dimension to mitigate the negative ecological footprint associated with manufacturing processes. Future research direction should underscore the need for green chemistry approaches to develop polymeric micelles for applications such as, Use the preparation methods manifest by solvent-free or aqueous-based preparations, which would obviate the need for hazardous organic solvents. Use biodegradable and biocompatible polymers from renewable sources. Use energy-efficient processing technologies to minimize carbon emissions associated with nanocarrier manufacture. These strategies will uphold the standards of sustainable

pharmaceutical development and respond to growing environmental demands from the healthcare sector.

Nanotechnology has considerable therapeutic potential; however, ensuring equitable access to cutting edge treatment is required. Careful consideration must be given to the ethical aspects of equitable access to advanced treatments, especially developing countries and low-resource settings, given the ramping burden of diseases such as IBD. Ethical considerations must include, Cost-effectiveness in the design and scale-up of nanotherapeutics. Technical exclusivity that leads to increased disparity in the health access of high income compared to low income populations. Collaboration with the regulatory bodies, regulatory systems, and patient advocacy groups to ensure developing nanomedicine considers accessibility in real world settings, cultural consideration, and health equity.

Bibliography

[1] M. Zeeshan, H. Ali, S. Khan, S. A. Khan, and B. Weigmann, "Advances in orally-delivered pH-sensitive nanocarrier systems; an optimistic approach for the treatment of inflammatory bowel disease," International journal of pharmaceutics, vol. 558, pp. 201-214, 2019.

[2] S. C. Ng et al., "Worldwide incidence and prevalence of inflammatory bowel disease in the 21st century: a systematic review of population-based studies," The Lancet, vol. 390, no. 10114, pp. 2769-2778, 2017.

[3] C. Yang and D. Merlin, "Nanoparticle-mediated drug delivery systems for the treatment of IBD: current perspectives," International journal of nanomedicine, pp. 8875-8889, 2019.

[4] R. Deshmukh, R. K. Harwansh, S. D. Paul, and R. Shukla, "Controlled release of sulfasalazine loaded amidated pectin microparticles through Eudragit S 100 coated capsule for management of inflammatory bowel disease," Journal of Drug Delivery Science and Technology, vol. 55, p. 101495, 2020.

[5] A. Karthikeyan et al., "Curcumin and its modified formulations on inflammatory bowel disease (IBD): the story so far and future outlook," Pharmaceutics, vol. 13, no. 4, p. 484, 2021.

[6] M. Vancamelbeke and S. Vermeire, "The intestinal barrier: a fundamental role in health and disease," Expert review of gastroenterology & hepatology, vol. 11, no. 9, pp. 821-834, 2017.

[7] E. Zarenezhad et al., "Protective role of flavonoids quercetin and silymarin in the viral-associated inflammatory bowel disease: An updated review," Archives of Microbiology, vol. 205, no. 6, p. 252, 2023.

[8] W. Liu et al., "Targeting strategies of oral nano-delivery systems for treating inflammatory bowel disease," International Journal of Pharmaceutics, vol. 600, p. 120461, 2021.

[9] T. Khare, S. S. Palakurthi, B. M. Shah, S. Palakurthi, and S. Khare, "Natural product-based nanomedicine in treatment of inflammatory bowel disease," International journal of molecular sciences, vol. 21, no. 11, p. 3956, 2020.

[10] F. Chen, Q. Liu, Y. Xiong, and L. Xu, "Current strategies and potential prospects of nanomedicine-mediated therapy in inflammatory bowel disease," International Journal of Nanomedicine, pp. 4225-4237, 2021.

[11] M. Zeeshan, Q. U. Ain, B. Weigmann, D. Story, B. R. Smith, and H. Ali, "Dual pH and microbial-sensitive galactosylated polymeric nanocargoes for multi-level targeting to combat ulcerative colitis," Asian Journal of Pharmaceutical Sciences, vol. 18, no. 4, p. 100831, 2023.

[12] S. S. Kesharwani, V. Jain, S. Dey, S. Sharma, P. Mallya, and V. A. Kumar, "An overview of advanced formulation and nanotechnology-based approaches for solubility and bioavailability enhancement of silymarin," Journal of Drug Delivery Science and Technology, vol. 60, p. 102021, 2020.

[13] S. Garg, M. Peeters, R. K. Mahajan, and P. Singla, "Loading of hydrophobic drug silymarin in pluronic and reverse pluronic mixed micelles," Journal of Drug Delivery Science and Technology, vol. 75, p. 103699, 2022.

[14] M. A. Tănase et al., "Mixed pluronic—Cremophor polymeric micelles as nanocarriers for poorly soluble antibiotics—The influence on the antibacterial activity," Pharmaceutics, vol. 13, no. 4, p. 435, 2021.

[15] V. Kumar et al., "Amphiphilic, lauric acid-coupled pluronic-based nano-micellar system for efficient glipizide delivery," Saudi Pharmaceutical Journal, vol. 32, no. 5, p. 102046, 2024. [Online]. Available: https://www.sciencedirect.com/science/article/pii/S1319016424000963?via

[16] M. U. Akbar, K. M. Zia, A. Nazir, J. Iqbal, S. A. Ejaz, and M. S. H. Akash, "Pluronic-based mixed polymeric micelles enhance the therapeutic potential of curcumin," Aaps Pharmscitech, vol. 19, pp. 2719-2739, 2018.

[17] K. Bhalodi, C. Kothari, and S. Butani, "Next-generation cancer nanotherapeutics: Pluronic® F127 based mixed micelles for enhanced drug delivery," Naunyn-Schmiedeberg's Archives of Pharmacology, pp. 1-30, 2024.

[18] N. Khaliq, J. Lee, S. Kim, D. Sung, and H. Kim, "Pluronic F-68 and F-127 based nanomedicines for advancing combination cancer therapy. Pharmaceutics. 2023; 15: 2102," ed.

[19] T. Woraphatphadung, W. Sajomsang, T. Rojanarata, T. Ngawhirunpat, P. Tonglairoum, and P. Opanasopit, "Development of chitosan-based pH-sensitive polymeric micelles containing curcumin for colon-targeted drug delivery," Aaps Pharmscitech, vol. 19, pp. 991-1000, 2018.

[20] X. Cai et al., "Colon-targeted delivery of tacrolimus using pH-responsive polymeric nanoparticles for murine colitis therapy," International journal of pharmaceutics, vol. 606, p. 120836, 2021.

[21] A. Abdollahy et al., "Therapeutic effect of 5-ASA and hesperidin-loaded chitosan/Eudragit® S100 nanoparticles as a pH-sensitive carrier for local targeted drug delivery in a rat model of ulcerative colitis," International Journal of Pharmaceutics, vol. 652, p. 123838, 2024.

[22] E. J. Heikal et al., "Development of Novel pH-sensitive eudragit coated beads containing curcumin-mesalamine combination for colon-specific drug delivery," Gels, vol. 9, no. 4, p. 264, 2023.

[23] S. S. Seoudi, E. A. Allam, A. H. El-Kamel, H. Elkafrawy, and R. M. El-Moslemany, "Targeted delivery of budesonide in acetic acid induced colitis: impact on miR-21 and E-cadherin expression," Drug Delivery and Translational Research, vol. 13, no. 11, pp. 2930-2947, 2023.

[24] M. Fallah et al., "Silymarin (milk thistle extract) as a therapeutic agent in gastrointestinal cancer," Biomedicine & Pharmacotherapy, vol. 142, p. 112024, 2021.

[25] M. Rastegarpanah et al., "A randomized, double blinded, placebo-controlled clinical trial of silymarin in ulcerative colitis," Chinese journal of integrative medicine, vol. 21, pp. 902-906, 2015.

[26] T.-H. T. Nguyen et al., "Improving silymarin oral bioavailability using silica-installed redox nanoparticle to suppress inflammatory bowel disease," Journal of controlled release, vol. 331, pp. 515-524, 2021.

[27] S. M. El-Hady, M. H. AbouGhaly, M. M. El-Ashmoony, H. S. Helmy, and O. N. El-Gazayerly, "Colon targeting of celecoxib nanomixed micelles using pulsatile drug delivery systems for the prevention of inflammatory bowel disease," International Journal of Pharmaceutics, vol. 576, p. 118982, 2020.

[28] A. R. Silva et al., "3-Carene-loaded poloxamer micelles against Leishmania: Development, characterization and in vitro proof-of-concept," Journal of Drug Delivery Science and Technology, vol. 82, p. 104376, 2023.

[29] N. U. Khaliq, J. Lee, S. Kim, D. Sung, and H. Kim, "Pluronic F-68 and F-127 based nanomedicines for advancing combination cancer therapy," Pharmaceutics, vol. 15, no. 8, p. 2102, 2023.

[30] X. Liu et al., "Development, characterization, and investigation of in vivo targeted delivery efficacy of luteolin-loaded, eudragit S100-coated mPEG-PLGA nanoparticles," AAPS PharmSciTech, vol. 23, no. 4, p. 100, 2022.

[31] Y. Liu et al., "Redox-sensitive Pluronic F127-tocopherol micelles: synthesis, characterization, and cytotoxicity evaluation," International journal of nanomedicine, pp. 2635-2644, 2017.

[32] P. Zarrintaj et al., "Poloxamer: A versatile tri-block copolymer for biomedical applications," Acta biomaterialia, vol. 110, pp. 37-67, 2020.

[33] R. Sareen, N. Jain, A. Rajkumari, and K. Dhar, "pH triggered delivery of curcumin from Eudragit-coated chitosan microspheres for inflammatory bowel disease: characterization and pharmacodynamic evaluation," Drug delivery, vol. 23, no. 1, pp. 55-62, 2016.

[34] A. M. Yousaf, U. R. Malik, Y. Shahzad, T. Mahmood, and T. Hussain, "Silymarin-laden PVP-PEG polymeric composite for enhanced aqueous solubility and dissolution rate: Preparation and in vitro characterization," Journal of pharmaceutical analysis, vol. 9, no. 1, pp. 34-39, 2019.

[35] W. Maryana, H. Rachmawati, and D. Mudhakir, "Formation of phytosome containing silymarin using thin layer-hydration technique aimed for oral delivery," Materials today: proceedings, vol. 3, no. 3, pp. 855-866, 2016.

[36] A. H. Ibrahim et al., "Formulation and optimization of lyophilized nanosuspension tablets to improve the physicochemical properties and provide immediate release of silymarin," International journal of pharmaceutics, vol. 563, pp. 217-227, 2019.

[37] J. Liang et al., "Chitosan-functionalized lipid-polymer hybrid nanoparticles for oral delivery of silymarin and enhanced lipid-lowering effect in NAFLD," Journal of nanobiotechnology, vol. 16, pp. 1-12, 2018.

[38] G. Yang, Y. Zhao, N. Feng, Y. Zhang, Y. Liu, and B. Dang, "Improved dissolution and bioavailability of silymarin delivered by a solid dispersion prepared using supercritical fluids," asian journal of pharmaceutical sciences, vol. 10, no. 3, pp. 194-202, 2015.

[39] S. Chaudhary, T. Garg, R. Murthy, G. Rath, and A. K. Goyal, "Development, optimization and evaluation of long chain nanolipid carrier for hepatic delivery of silymarin through lymphatic transport pathway," International journal of pharmaceutics, vol. 485, no. 1-2, pp. 108-121, 2015.

[40] S. S. Nasr, M. M. Nasra, H. A. Hazzah, and O. Y. Abdallah, "Mesoporous silica nanoparticles, a safe option for silymarin delivery: Preparation, characterization, and in vivo evaluation," Drug Delivery and Translational Research, vol. 9, pp. 968-979, 2019.

[41] A. Nagi, B. Iqbal, S. Kumar, S. Sharma, J. Ali, and S. Baboota, "Quality by design based silymarin nanoemulsion for enhancement of oral bioavailability," Journal of Drug Delivery Science and Technology, vol. 40, pp. 35-44, 2017.

[42] V. Piazzini, C. Rosseti, E. Bigagli, C. Luceri, A. R. Bilia, and M. C. Bergonzi, "Prediction of permeation and cellular transport of Silybum marianum extract formulated in a nanoemulsion by using PAMPA and Caco-2 cell models," Planta medica, vol. 83, no. 14/15, pp. 1184-1193, 2017.

[43] N.-T. Tung et al., "Formulation and biopharmaceutical evaluation of supersaturatable self-nanoemulsifying drug delivery systems containing silymarin," International journal of pharmaceutics, vol. 555, pp. 63-76, 2019.

[44] M. El-Far, N. Salah, A. Essam, A. O. Abd El-Azim, and I. M. El-Sherbiny, "Silymarin nanoformulation as potential anticancer agent in experimental Ehrlich ascites carcinoma-bearing animals," Nanomedicine, vol. 13, no. 15, pp. 1865-1858, 2018.

[45] E. İspir, M. İnal, Z. Gün Gök, and M. Yiğitoğlu, "Synthesis, characterization and in vitro release analysis of pluronic F127 copolymer micelles containing quercetin as a hydrophobic drug," Polymer Bulletin, vol. 81, no. 8, pp. 6801-6822, 2024.

[46] N. T. Dintcheva et al., "Pluronic nanoparticles as anti-oxidant carriers for polymers," Polymer Degradation and Stability, vol. 134, pp. 194-201, 2016.

[47] P. Dehghan Kelishady, E. Saadat, F. Ravar, H. Akbari, and F. Dorkoosh, "Pluronic F127 polymeric micelles for co-delivery of paclitaxel and lapatinib against metastatic breast cancer: preparation, optimization and in vitro evaluation," Pharmaceutical development and technology, vol. 20, no. 8, pp. 1009-1017, 2015.

[48] J. Magalhães, L. L. Chaves, A. C. Vieira, S. G. Santos, M. Pinheiro, and S. Reis, "Optimization of rifapentine-loaded lipid nanoparticles using a quality-by-design strategy," Pharmaceutics, vol. 12, no. 1, p. 75, 2020.

[49] M. Zeeshan et al., "A holistic QBD approach to design galactose conjugated PLGA polymer and nanoparticles to catch macrophages during intestinal inflammation," Materials Science and Engineering: C, vol. 126, p. 112183, 2021.

[50] M. Zeeshan, H. Ali, S. Khan, M. Mukhtar, M. I. Khan, and M. Arshad, "Glycyrrhizic acid-loaded pH-sensitive poly-(lactic-co-glycolic acid) nanoparticles for the amelioration of inflammatory bowel disease," Nanomedicine, vol. 14, no. 15, pp. 1945-1969, 2019.

[51] M. Ghezzi et al., "Polymeric micelles in drug delivery: An insight of the techniques for their characterization and assessment in biorelevant conditions," Journal of Controlled Release, vol. 332, pp. 312-336, 2021.

[52] N. A. Hanafy and M. A. El-Kemary, "Silymarin/curcumin loaded albumin nanoparticles coated by chitosan as muco-inhalable delivery system observing anti-inflammatory and anti COVID-19 characterizations in oleic acid triggered lung injury and in vitro COVID-19 experiment," International journal of biological macromolecules, vol. 198, pp. 101-110, 2022.

[53] A. E. El-Nahas, A. N. Allam, D. A. Abdelmonsif, and A. H. El-Kamel, "Silymarin-loaded eudragit nanoparticles: formulation, characterization, and hepatoprotective and toxicity evaluation," Aaps Pharmscitech, vol. 18, pp. 3076-3086, 2017.